IC/86/356
INTERNAL REPORT
(Limited distribution)

International Atomic Energy Agency
and
United Nations Educational Scientific and Cultural Organization
INTERNATIONAL CENTRE FOR THEORETICAL PHYSICS

SPIN FLIP INELASTIC SCATTERING IN ELECTRON ENERGY LOSS SPECTROSCOPY OF A FERROMAGNETIC METAL *

C.J. Bocchetta, E. Tosatti and S. Yin **
International Centre for Theoretical Physics, Trieste, Italy
and
International School for Advanced Studies, Trieste, Italy.

ABSTRACT

A model ferromagnetic metal is used to calculate the spin-polarization which occurs during inelastic electron-metal scattering with the production of an electron-hole pair. The polarization is found to have contributions from unequal spin-flip as well as non-flip energy loss rates. Our results indicate an asymmetry of the order of a few percent with parameters roughly modelling iron.

MIRAMARE - TRIESTE
November 1986

* To be submitted for publication.

** Permanent address: Department of Physics, Arts and Science University, Rangoon, Burma.

I. INTRODUCTION

Spin polarized electron energy loss spectroscopy (SPEELS) can now be considered a valuable technique for studying both the bulk and surface electronic structures of ferromagnetic metals [1-4]. Much physical information on the properties of a ferromagnet is contained in the spectrum of elementary excitations of the system (particularly the spin up (triplet) excitations; Stoner excitations, spin waves). Due to the imbalance between the majority-spin density and the minority-spin density, spin polarized electron energy loss processes turn out to be strongly spin dependent. With the use of SPEELS it is now possible to study the Stoner continuum and the $\omega(q)$ of modes therein. The asymmetry measured in a typical spin polarized electron energy loss experiment gives the amount of inelastic exchange scattering that has occurred. This is because an asymmetry in the inelastic scattering means spin-flip processes, but spin-flip can only occur in an electron system via spin exchange, i.e. an up (down) spin electron exchanges with an opposite spin electron. It is the purpose of this paper to present the basic equations used by a theory [5-6], dealing with electron metal scattering that accounts for electron exchange processes in SPEELS. We shall exclude from our considerations any effects of spin-orbit coupling, which can produce spin polarization even in a paramagnetic metal [7]. Spin orbit effects are effectively removed from energy loss spectroscopy (ELS) data by reversing the magnetization of the sample.

In SPEELS the impinging electrons can lose energy by exciting magnons plasmons and electron-hole pairs (disregarding electron-phonon scattering as very weak). Magnon excitation is clearly spin-dependent [8]. It has however never been clearly pin-pointed experimentally. Various estimates show that its integrated contribution to ELS should be smaller than other excitations for the energies considered here [9,10]. Plasmons in a ferromagnetic metal are collective excitations simultaneously involving majority and minority spin electrons. It seems plausible that the energy loss process due to plasmons should also be approximately spin-independent: This point has been considered by Helman and Baltensperger [11] and the spin independence has been verified by experimental observation [12]. This leaves electron hole (Stoner) excitations as the process which is mainly responsible for the spin-dependence of the ELS process in ferromagnetic metals. There are basically two contributions to spin polarization from such electron-hole pairs. Firstly, the possibility of an up spin electron to lose energy and remain up becomes different from that of a down spin electron to lose the same energy and remain down. Secondly, there is the effect of spin-flip loss events. These events occur even in a paramagnetic metal where they can easily be of the same importance as the non-flip transitions. In this case, though, $n_\uparrow = n_\downarrow$ and their net effect balances out and can only

become detectable if both incoming and outgoing spin polarizations can be measured simultaneously. In the ferromagnetic case this balance is destroyed and spin-flip inelastic events will contribute to ELS polarization. In what follows we shall be concerned with the calculation of the two inelastic non-flip probabilities, $R^{\uparrow}_{nf}(E_0,\omega)$ and $R^{\downarrow}_{nf}(E_0,\omega)$, as well as the corresponding spin-flip probabilities $R^{\uparrow}_{f}(E_0,\omega)$ and $R^{\downarrow}_{f}(E_0,\omega)$, (in this latter notation, $\uparrow$ or $\downarrow$ stands for the incoming electron spin orientation and f stands for flip, so that for example $R^{\downarrow}_{f}(E_0,\omega)$ is the probability that an incoming electron with energy E_0 and a spin-down orientation, will loss energy ω and flip to spin up).

We shall present in the following sections our model calculations for the spin-flip and non-flip transitions which can occur when SPEELS is applied to a ferromagnetic metal. Our work represents an extreme idealization of the real process and its basic purpose is qualitative. Surfaces are neglected throughout, and a continuous infinite electron system described by a band model replaces the real metal. Two extremely simplified band models will be defined and parameters chosen in order to model iron very roughly for two energy regions of the incoming electron. That is, low energy (E_0 < 5 eV, Model A) and high energy (5 eV < E_0 < 200 eV, Model B) primary electrons. In Sec. II, we describe our method of calculation and apply it initially to a paramagnetic metal. In Sec. III the two models of a prototype ferromagnetic metal are defined and the four loss rates ($R^{\downarrow}_{nf}$, $R^{\uparrow}_{nf}$, $R^{\downarrow}_{f}$, $R^{\uparrow}_{f}$) are calculated. Finally the results are collected and discussed in Sec. IV.

II. ENERGY LOSS RATES FOR SPIN-FLIP AND NON-FLIP SCATTERING PROCESSES IN A PARAMAGNETIC METAL

2.1 Spin-flip scattering in a paramagnetic metal

Spin-flip, without spin-orbit coupling effects, occurs when an incoming primary spin-polarized low energy electron falls into one of the empty states above E_F and kicks out an opposite-sign electron from one of the filled bands. This is illustrated diagramatically in Fig.1a.

Our starting model is simply a free-electron-metal of electron density n, Fermi energy E_F, and work function ϕ. For all future numerical estimates we shall assume $n = 1.7 \times 10^{23}$ cm^{-3}, a corresponding Fermi energy is $E_F = 11.1$ eV, and a work function is about $\phi = 4.3$ eV. These numbers correspond very crudely to the case of Al (and of Fe). The primary electron energy E_0 will be measured with respect to the vacuum zero, which is $E_F + \phi$, above the bottom of the band.

We calculate the energy loss rate due to the spin-flip scattering process, $R^{\downarrow}_{f}(\omega)$, for an incoming spin-down electron by means of perturbation theory (Green's functions). The scattering rate of the electron from the state $\underline{p}\downarrow, E(p)$ to the final state $(\underline{p}-\underline{q})\uparrow$, $E(p)-\omega$ with the momentum transfer $\underline{q}$ and energy transfer ω between antiparallel spin electrons is proportional to the imaginary part of the forward scattering amplitude, that is according to Fig.1b [13]:

$$R^{\downarrow}_{f}(\omega) = -\frac{2}{\pi}\,\mathrm{Im}\left\{ i^2(-1)\int\frac{d^3q}{(2\pi)^3}\int\frac{d^3k}{(2\pi)^3}\int\frac{d\epsilon}{2\pi}\,\left|V(\underline{p}-\underline{q}-\underline{k}, E(\underline{p})-\epsilon-\omega)\right|^2 \right.$$
$$\left. \times\, G((\underline{p}-\underline{q})\uparrow, E(p)-\omega)\, G((\underline{q}+\underline{k})\downarrow, \epsilon+\omega)\, G(\underline{k}\uparrow, \epsilon)\right\}. \qquad (1)$$

Here we have taken $\hbar = 1$ and ω as a positive quantity always. $G(k\uparrow,\epsilon)$ is the single particle Green's function of the metal, for bound states labelled by momentum k, energy ϵ and spin $\uparrow$. V represents the Coulomb potential. Substituting the free electron Green's functions in Eq.(1), we obtain

$$R^{\downarrow}_{f}(\omega) = -\frac{2}{\pi}\,\mathrm{Im}\left\{\int\frac{d^3q}{(2\pi)^3}\int\frac{d^3k}{(2\pi)^3}\int\frac{d\epsilon}{(2\pi)}\,\left|V(\underline{p}-\underline{q}-\underline{k}, E(\underline{p})-\epsilon-\omega)\right|^2 \right.$$
$$\left. \times\, \frac{\theta(E(\underline{p}-\underline{q})\uparrow - E_f-\phi)}{(E(\underline{p})\downarrow-\omega-E(\underline{p}-\underline{q})\uparrow+i\eta)}\cdot\frac{\theta(E(\underline{q}+\underline{k})\downarrow - E_f)}{(\epsilon+\omega-E(\underline{q}+\underline{k})\downarrow+i\eta)}\cdot\frac{\theta(E_f-E(\underline{k})\uparrow)}{(\epsilon-E(\underline{k})\uparrow-i\eta)}\right\} \qquad (2)$$

Here $\theta(E(\underline{p}-\underline{q})\uparrow - E_F - \phi)$ ensures the outgoing spin-flipped electron to be above the vacuum level. $\theta(E(\underline{q}+\underline{k})\downarrow - E_F)$ restricts the incoming electron to fall down into the energy band above E_F and $\theta(E_F - E(\underline{k})\uparrow)$ restricts the hole $(\underline{k})$ to be below E_F. Even the first integration is in general difficult, due to the complex ϵ-dependence contained in the dynamically screened potential V. As a first approximation we shall replace V with a statically screened Coulomb interaction, namely

$$V(\underline{q}) = \frac{V(\underline{q})}{\mathcal{E}(\underline{q})} \simeq \frac{4\pi e^2}{q^2+q_{FT}^2} \qquad (3)$$

where q_{FT} is the Fermi-Thomas static screening length given by

$$q_{fb} = 3^{1/2}\frac{\omega_p}{v_f} = 3^{1/2}\frac{(4\pi n e^2/m)^{1/2}}{p_f/m} \qquad (4)$$

Then the energy integration in Eq.(2) can be done by straightforward contour integration since the two terms have poles on the opposite sides of the real axis. Thus one obtains, after ϵ-integration and taking the imaginary part,

$$R^{\downarrow}_f(\omega) = 2\pi\int\frac{d^3q}{(2\pi)^3}\int\frac{d^3k}{(2\pi)^3}\,\theta(E(\underline{p}-\underline{q})\uparrow - E_f-\phi)\,\theta(E(\underline{q}+\underline{k})\downarrow - E_f)$$

$$\times\,\theta(E_f - E(\underline{k})\uparrow)\,|V(\underline{p}-\underline{q}-\underline{k})|^2\,\delta(E(\underline{p})\downarrow - E(\underline{p}-\underline{q})\uparrow - \omega)$$

$$\times\,\delta(E(\underline{q}+\underline{k})\downarrow - E(\underline{k})\uparrow - \omega) \qquad (5)$$

It should be noted that in our free-electron model $E(p) = p^2/2m$, $\theta(E(q+k)-E_F) = \theta(|q+k|-p_F)$ and $\theta(E_F-E(k)) = \theta(p_F-|k|)$. Using dimensionless quantities where all momenta are expressed in terms of $p_F^{\uparrow}$, i.e. $q \to q/p_F^{\uparrow}$, and all energies are expressed in terms of $2E_F$, $\omega \to \omega/2E_F$, Eq.(5) can be expressed in a simpler form as follows:

$$R^{\downarrow}_f(\omega) = \frac{1}{2\pi^3}\left(\frac{e^2P_f^{\uparrow}}{2E_f}\right)^2\int d^3q\int d^3k\;\theta(E(\underline{p}-\underline{q})\uparrow - E_f-\phi)\,\theta(1-k^{\uparrow})$$

$$\times\,\frac{\theta(|q+k|\downarrow - 1)\;\delta(\underline{p}\cdot\underline{q}-q^2/2-\omega)\,\delta(\underline{k}\cdot\underline{q}+q^2/2-\omega)}{((\underline{p}-\underline{q}-\underline{k})^2 + q_{fb}^2)^2} \qquad (6)$$

The details of the integrations involved with Eq.(6) and of all the others discussed in this paper can be found in the Appendix. The resulting spin-flip rate is shown in Figs.2 and 3. Note that for a paramagnetic metal, spin-flip loss rates for incoming spin up and spin down electrons are equal.

2.2 Non-flip scattering in a paramagnetic metal

The possible electron-hole pair excitation processes contributing to non-flip energy loss inelastic scattering of an incoming spin-down electron are shown in Fig.4.

We denote by $R^{\downarrow}_{nf1}(\omega)$ the non-flip transition rate associated with Fig.4a. This represents the process in which an incoming spin-down electron loses energy by exciting either down or up spin electron-hole pairs with equal probability (i.e. Figs.4b and 4b'). $R^{\downarrow}_{nf1}(\omega)$ is given by

$$R^{\downarrow}_{nf1}(\omega) = -\frac{2}{\pi}\,\mathrm{Im}\left\{i^2(-1)\int\frac{d^3q}{(2\pi)^3}\int\frac{d^3k}{(2\pi)^3}\int\frac{d\epsilon}{2\pi}\,|V(q)|^2\right.$$

$$\left.\times\,\frac{\theta(E(p-q)\downarrow - E_f-\phi)}{(E(\underline{p})\downarrow - \omega - E(\underline{p}-\underline{q})\downarrow + i\eta)}\cdot\frac{\theta(E(\underline{q}+\underline{k})\downarrow - E_f)}{(\epsilon+\omega-E(\underline{q}+\underline{k})\downarrow + i\eta)}\cdot\frac{\theta(E_f - E(k)\downarrow)}{(\epsilon - E(\underline{k})\downarrow - i\eta)}\right\}$$

$$= 2\pi\int\frac{d^3q}{(2\pi)^3}\int\frac{d^3k}{(2\pi)^3}\,|V(q)|^2\,\theta(E(\underline{p}-\underline{q})\downarrow - E_f-\phi)\,\theta(E(\underline{q}+\underline{k})\downarrow - E_f)$$

$$\times\,\theta(E_f - E(\underline{k})\downarrow)\,\delta(E(\underline{p})\downarrow - E(\underline{p}-\underline{q})\downarrow - \omega)\,\delta(E(\underline{q}+\underline{k})\downarrow - E(\underline{k})\downarrow - \omega)$$

$$= \frac{1}{2\pi^3}\left(\frac{e^2P_f^{\uparrow}}{2E_f}\right)^2\int d^3q\int d^3k\;\frac{\theta(E(\underline{p}-\underline{q})\downarrow - E_f-\phi)}{(q^2+q_{fb}^2)^2}\cdot\theta(|\underline{q}+\underline{k}|-1)$$

$$\times\;\theta(1-k)\cdot\delta(\underline{p}\cdot\underline{q}-q^2/2-\omega)\,\delta(\underline{q}\cdot\underline{k}+q^2/2-\omega) \qquad (7)$$

The last expression in Eq.(7) is in terms of dimensionless quantities.

There are three diagrams associated with the non-flip transition process as shown in Fig.4c in which the incoming spin-down electron falls into the band above E_F and kicks out the spin-down electron from the same band below E_F. These are the exchange processes. Let us call $R^{\downarrow}_{nf2}(\omega)$ the transition rate associated with the diagram in Fig.4d. This is very similar to the process, Fig.1b, previously considered. We give the final expression of $R^{\uparrow}_{nf2}(\omega)$ as follows:

$$R^{\downarrow}_{nf2}(\omega) = \frac{1}{2\pi^3}\left(\frac{e^2P_f^{\uparrow}}{2E_f}\right)^2\int d^3q\int d^3k\;\frac{\theta(E(\underline{p}-\underline{q})\downarrow - E_f-\phi)}{((\underline{p}-\underline{q}-\underline{k})^2+q_{fb}^2)^2}$$

$$\times\,\theta(1-k)\,\theta(|\underline{q}+\underline{k}|-1)\,\delta(\underline{p}\cdot\underline{q}-q^2/2-\omega)\,\delta(\underline{q}\cdot\underline{k}+q^2/2-\omega) \qquad (8)$$

Denoting by $R^{\downarrow}_{nf3}(\omega)$ the transition rate associated with Figs.4e and 4f, we can write

$$R^{\downarrow}_{nf3}(\omega) = -\frac{1}{2\pi^3}\left(\frac{e^2 p_f^{\uparrow}}{2E_f}\right)^2 \int d^3q \int d^3k \;\theta(E(\underline{p}-\underline{q})\downarrow - E_f - \phi)$$

$$\times \;\frac{\theta(1-k)\,\theta(|\underline{q}+\underline{k}|-1)\,\delta(\underline{p}\cdot\underline{q} - q^2/2 - \omega)\,\delta(\underline{q}\cdot\underline{k} - q^2/2 - \omega)}{(q^2 + q_{fc}^2)((\underline{p}-\underline{q}-\underline{k})^2 + q_{fc}^2)} \qquad (9)$$

The two figures e and f associated with the exchange process contribute equally to the scattering amplitude by the amount given in Eq.(9). Note that this quantity is of opposite sign to the others. The total non-flip transition rate for an incoming spin-down electron can be obtained by summing up these contributions. Thus one obtains

$$R^{\downarrow}_{nf}(\omega) = 2R^{\downarrow}_{nf1}(\omega) + R^{\downarrow}_{nf2}(\omega) + 2R^{\downarrow}_{nf3}(\omega) \qquad (10)$$

It is also to be noted that in the present case $R^{\downarrow}_{nf}(\omega) = R^{\uparrow}_{nf}(\omega)$. The quantity $R^{\downarrow}_{f}(\omega)$ of Eq.(6) and $R^{\downarrow}_{nf}(\omega)$ of Eq.(10) are to be compared for a given electron energy loss ω. The results will be discussed in detail in Sec.IV.

III. THE FERROMAGNETIC CASE (TWO-BAND MODELS)

In the spirit of the preceeding section we now formulate the required partial flip/non-flip scattering amplitudes for a ferromagnetic system. Ideally one would like to use a realistic band structure for a ferromagnetic, for example iron [14; see also Fig.7 in Ref.15]. Unfortunately, such a calculation is for the moment out of the question. Since we are essentially looking for qualitative (gross) results we consider the main features of the band structure of iron [14]. We note the following facts, firstly: near E_F there are two sets of very flat d-bands, one above and one below the Fermi energy, with an exchange splitting of 2.0 eV. Secondly, very high above E_F (5 eV or more), the bands are more free-electron like and the exchange splitting seems reduced. In view of this we consider two models A and B, that should be appropriate when $E_0 < 5$ eV and when $E_0 > 5$ eV, respectively.

Model A: This model has flat bands of which only the lowest is occupied by spin up electrons. The exchange splitting between the bands is $\Delta = 2$ eV. The Fermi energy E_F is 1 eV measured from the bottom of the lower band. The effective mass m^* of the electron in this band is given by $m^*/m = 18$, with this choice, the Fermi momentum $p_F \simeq 2.2\ \text{Å}^{-1}$, which is in turn close to the Brillouin zone of Fe.

Model B: Here both bands are occupied with an exchange splitting Δ between them. We assume that both bands have the same Fermi energy. Let $p_F^{\uparrow}$ be the Fermi momentum of the spin up band, and $p_F^{\downarrow}$ for the spin down band. We now choose Δ as a parameter defining the amount of magnetization. Using the fact that $p_F^{\downarrow}/p_F^{\uparrow} = (1-\Delta/E_F)^{1/2}$ and $p_F^{\uparrow}(\downarrow) \alpha [n^{\uparrow(\downarrow)}]^{1/3}$, where n is the number of up (down) spin electrons, we obtain

$$P_B = \frac{n^{\uparrow} - n^{\downarrow}}{n^{\uparrow} + n^{\downarrow}} = \frac{1 - (1 - \Delta/E_f)^{2/3}}{1 + (1 - \Delta/E_f)^{2/3}} \qquad (11)$$

which defines the amount of bulk magnetization. Use of Eq.(11) shows that *no single* value of Δ will give the true value of P_B for iron. As mentioned above, we are basically looking for qualitative results, thus we will choose $\Delta = 1.5$ eV, $E_F = 11.93$ eV and $m^* = m$.

3.1 Spin-flip rate calculation for Model A

We consider first an incoming spin-down electron, It will fall down into the empty spin-down band and kick out another electron in the spin-up band, as shown in Fig.5a. Following the same procedure discussed in Sec.II, the spin-flip transition rate $R^{\downarrow}_{f}(\omega)$ associated with Fig.5b, for Model A is obtained as

$$R^{\downarrow}_{f}(\omega) = -\frac{2}{\pi} \mathrm{Im} \left\{ i^2(-1) \int \frac{d^3q}{(2\pi)^3} \int \frac{d^3k}{(2\pi)^3} \int \frac{d\epsilon}{2\pi} \;|V(\underline{p}-\underline{q}-\underline{k})|^2 \right.$$

$$\left. \times \frac{\theta(E(p-q)\uparrow - E_f - \phi)}{(E(\underline{p})\downarrow - \omega - E(\underline{p}-\underline{q})\uparrow + i\eta)} \cdot \frac{\theta(E(\underline{q}+\underline{k})\downarrow - \Delta)}{(\epsilon + \omega - E(\underline{q}+\underline{k})\downarrow + i\eta)} \cdot \frac{\theta(E_f - E(\underline{k})\uparrow)}{(\epsilon - E(\underline{k})\uparrow - i\eta)} \right\}$$

$$= 2\pi \int \frac{d^3q}{(2\pi)^3} \int \frac{d^3k}{(2\pi)^3} \;|V(\underline{p}-\underline{q}-\underline{k})|^2\, \theta(E(\underline{p}-\underline{q})\uparrow - E_f - \phi)\, \theta(E(\underline{q}+\underline{k}) - \Delta)$$

$$\times \theta(E_f - E(\underline{k})\uparrow)\, \delta(E(\underline{p})\downarrow - E(\underline{p}-\underline{q})\uparrow - \omega)\, \delta(E(\underline{q}+\underline{k}) - E(\underline{k})\uparrow - \omega) \qquad (12)$$

In this model $E(p)\downarrow = p^2/2m + \Delta$ and $E(p)\uparrow = p^2/2m$, measuring from the bottom of the lower band. Here also we impose static screening on the Coulomb interaction $V(\underline{p}-\underline{q}-\underline{k})$. Again using dimensionless quantities for energies and momenta, one can write

$$\delta(E(\underline{p})\downarrow - E(\underline{p}-\underline{q})\uparrow - \omega) = \delta(\underline{p}\cdot\underline{q} - q^2/2 + \Delta - \omega)$$

$$\delta(E(\underline{q}+\underline{k})\downarrow - E(\underline{k})\uparrow - \omega) = \delta(\underline{q}\cdot\underline{k} + q^2/2 + \Delta - \omega)$$

$$\theta(E_f - E(\underline{k})\uparrow) = \theta(1-k) \qquad (13)$$

Eq.(12) can then be rewritten in the following form:

$$R^{\downarrow}_f(\omega) = \frac{1}{2\pi^3}\left(\frac{e^2 p_f^{\uparrow}}{2E_f}\right)^2 \int d^3q \int d^3k \, \frac{\theta(E(\underline{p}-\underline{q})\uparrow - \epsilon_f - \phi)\,\theta(E(\underline{q}+\underline{k})\downarrow - \Delta)}{((\underline{p}-\underline{q}-\underline{k})^2 + q_{fc}^2)^2}$$

$$\times\, \theta(1-k)\,\delta(\underline{p}\cdot\underline{q} - q^2/2 + \Delta - \omega)\,\delta(\underline{q}\cdot\underline{k} + q^2/2 + \Delta - \omega) \qquad (14)$$

As before $\theta(E(p-q)\uparrow - E_F - \phi)$ ensures that the outgoing spin flipped electron be above the vacuum zero. After integration with $\delta(E(p))\downarrow - E(p-q)\uparrow - \omega)$ it becomes $\theta(E(p)\downarrow - E_F - \phi - \omega)$ and sets the minimum threshold energy of the incoming electron, namely $E_{0,min} = E(p)\downarrow - E_F - \phi = \omega$. Also the condition $\theta(E(q+k)\downarrow - \Delta)$ ensures that the incoming electron falls into the empty spin-down band Δ above the bottom of the spin-up band. After integration with $\delta(E(q+k)\downarrow - E(k)\uparrow - \omega)$ it becomes $\theta(E(k)\uparrow - \omega - \Delta)$, and since the maximum value of $E(k)$ is E_F, this condition sets the minimum threshold energy loss to be $\omega_{min} = \Delta - E_F$. Here k integration is restricted in the Fermi sphere of radius 1. However no restriction is needed for $|\underline{q}+\underline{k}|$ to be outside the Fermi sphere because the spin-down band is already empty.

3.2 Non-flip rate calculation for Model A

Non-flip transition processes associated with the electron-hole excitations for an incoming spin-down electron are shown in Fig.5c. Denoting $R^{\downarrow}_{nf}(\omega)$ for the non-flip transition rate associated with this process for fixed energy loss ω, the final expression for $R^{\downarrow}_{nf}(\omega)$ is,

$$R^{\downarrow}_{nf}(\omega) = -\frac{2}{\pi}\,\mathrm{Im}\left\{ i^2(-1)\int\frac{d^3q}{(2\pi)^3}\int\frac{d^3k}{(2\pi)^3}\int\frac{d\epsilon}{2\pi}\;|V(q)|^2\right.$$

$$\left.\times\,\frac{\theta(E(\underline{p}-\underline{q})\downarrow - E_f - \phi)}{(E(\underline{p})\downarrow - \omega - E(\underline{p}-\underline{q})\downarrow + i\eta)}\,\frac{\theta(E(\underline{q}+\underline{k})\uparrow - E_f)}{(\epsilon+\omega-E(\underline{q}+\underline{k})\uparrow + i\eta)}\,\frac{\theta(E_f - E(\underline{k})\uparrow)}{(\epsilon - E(\underline{k})\uparrow - i\eta)}\right\}$$

$$= 2\pi\int\frac{d^3q}{(2\pi)^3}\int\frac{d^3k}{(2\pi)^3}\;|V(q)|^2\,\theta(E(\underline{p}-\underline{q})\downarrow - E_f - \phi)\,\theta(E(\underline{q}+\underline{k})\uparrow - E_f)$$

$$\times\,\theta(E_f - E(\underline{k})\uparrow)\,\delta(E(\underline{p})\downarrow - E(\underline{p}-\underline{q})\downarrow - \omega)\,\delta(E(\underline{q}+\underline{k})\uparrow - E(\underline{k})\uparrow - \omega)\,. \qquad (15)$$

Using dimensionless quantities for the energies and momenta, one can express

$$\delta(E(\underline{p})\downarrow - E(\underline{p}-\underline{q})\downarrow - \omega) = \delta(\underline{p}\cdot\underline{q} - q^2/2 - \omega)$$

$$\delta(E(\underline{q}+\underline{k})\uparrow - E(\underline{k})\uparrow - \omega) = \delta(\underline{q}\cdot\underline{k} + q^2/2 - \omega)$$

$$\theta(E_f - E(\underline{k})\uparrow) = \theta(1-k)\,. \qquad (16)$$

Eq.(15) can now be rewritten in the following form:

$$R^{\downarrow}_{nf}(\omega) = \frac{1}{2\pi^3}\left(\frac{e^2 p_f^{\uparrow}}{2E_f}\right)^2 \int d^3q \int d^3k \, \frac{\theta(E(\underline{p}-\underline{q})\downarrow - E_f - \phi)}{(q^2 + q_{fc}^2)^2}$$

$$\times\,\theta(|\underline{q}+\underline{k}|-1)\,\theta(1-k)\,\delta(\underline{p}\cdot\underline{q} - q^2/2 - \omega)\,\delta(\underline{q}\cdot\underline{k} + q^2/2 - \omega)\,. \qquad (17)$$

Eq.(17) is very similar to Eq.(7) except that here the incoming and outgoing electrons are in the spin-down band which is Δ above the spin-up band where the electron hole excitation has taken place.

Next, we consider an incoming spin-up electron. For this the only possible processes are non-flip scattering events. The relevant interactions associated with these non-flip processes are exactly the same as those given in Fig.4, excluding Fig.4b', with spin direction reversed. Thus we can use the same equations (7), (8) and (9) and the final form of $R^{\uparrow}_{nf}(\omega)$ is,

$$R^{\uparrow}_{nf}(\omega) = R^{\uparrow}_{nf1}(\omega) + R^{\uparrow}_{nf2}(\omega) + 2R^{\uparrow}_{nf3}(\omega) \qquad (18)$$

3.3. Spin-flip rate calculation for Model B

Let us first consider the spin-flip process for an incoming spin-down electron. The possible scattering process is shown in Fig.6a. The final expression for this spin-flip scattering rate $R^{\downarrow}_{f}(\omega)$ can be given in dimensionless units as

$$R^{\downarrow}_{f}(\omega) = \frac{1}{2\pi^3}\left(\frac{e^2 P^{\uparrow}_{f}}{2E_f}\right)^2 \int d^3q \int d^3k \, \frac{\theta(E(\underline{p}-\underline{q})\uparrow - E_f - \phi)\,\theta(1-k)}{((\underline{p}-\underline{q}-\underline{k})^2 + q^2_{fc})^2}$$

$$\times \theta(|\underline{q}+\underline{k}| - (1-2\Delta)^{1/2})\,\delta(\underline{p}\cdot\underline{q} - q^2/2 + \Delta - \omega)\,\delta(\underline{q}\cdot\underline{k} + q^2/2 + \Delta - \omega) \qquad (19)$$

It should be noted that when performing the k integration, k must be restricted to the interior of the Fermi sphere ($k < 1$), while the vector $(\underline{q}+\underline{k})$ must always be greater than $(1-2\Delta)^{1/2}$.

For an incoming spin-up electron the possible spin-flip process is shown in Fig.6c. Here the incoming spin-up electron falls into the spin-up band above E_f and kicks out a spin-down electron. Denoting $R^{\uparrow}_{f}(\omega)$ for the spin-flip transition rate for this process, and following the above procedure, the final expression for the integral is

$$R^{\uparrow}_{f}(\omega) = \frac{1}{2\pi^3}\left(\frac{e^2 P^{\uparrow}_{f}}{2E_f}\right)^2 \int d^3q \int d^3k \, \frac{\theta(E(\underline{p}-\underline{q})\downarrow - E_f - \phi)\,\theta(|\underline{q}+\underline{k}|-1)}{((\underline{p}-\underline{q}-\underline{k})^2 + q^2_{fc})^2}$$

$$\times \theta((1-2\Delta)^{1/2} - k)\,\delta(\underline{p}\cdot\underline{q} - q^2/2 - \Delta - \omega)\,\delta(\underline{q}\cdot\underline{k} + q^2/2 - \Delta - \omega) \qquad (20)$$

3.4 Non-flip rate calculation for Model B

We first consider the case when the incoming electron is spin-down. The possible non-flip scattering processes are shown in Fig.7. For the process $R^{\downarrow}_{nf1}$ of Fig.7a, and associated Feynman diagram, Fig.7b, the incoming spin-down electron loses energy by exciting an electron-hole pair in the spin-down band. There is no contribution from the spin-up band in this case.

For the process $R^{\downarrow}_{nf2}$ shown in Fig.7c and the related diagram Fig.7d, the incoming spin-down electron excites an electron-hole pair in the spin-up band. Processes $R^{\downarrow}_{nf3}$ and $R^{\downarrow}_{nf4}$ shown in Fig.7e and the related diagrams Fig.5 (7f, 7g, 7h) describe a spin-down electron falling into the spin-down band above E_F, and ejecting another electron from the same band below E_F. The final expressions for these scattering rates in terms of dimensionless quantities are

$$R^{\downarrow}_{nf1}(\omega) = \frac{1}{2\pi^3}\left(\frac{e^2 P^{\uparrow}_{f}}{2E_f}\right)^2 \int d^3q \int d^3k \, \frac{\theta(E(\underline{p}-\underline{q})\downarrow - E_f - \phi)\,\theta((1-2\Delta)^{1/2} - k)}{(q^2 + q^2_{fc})^2}$$

$$\times \theta(|\underline{q}+\underline{k}| - (1-2\Delta)^{1/2})\,\delta(\underline{p}\cdot\underline{q} - q^2/2 - \omega)\,\delta(\underline{q}\cdot\underline{k} + q^2/2 - \omega) \qquad (21)$$

$$R^{\downarrow}_{nf2}(\omega) = \frac{1}{2\pi^3}\left(\frac{e^2 P^{\uparrow}_{f}}{2E_f}\right)^2 \int d^3q \int d^3k \, \frac{\theta(E(\underline{p}-\underline{q})\downarrow - E_f - \phi)\,\theta(1-k)}{(q^2 + q^2_{fc})^2}$$

$$\times \theta(|\underline{q}+\underline{k}| - 1)\,\delta(\underline{p}\cdot\underline{q} - q^2/2 - \omega)\,\delta(\underline{q}\cdot\underline{k} + q^2/2 - \omega) \qquad (22)$$

$$R^{\downarrow}_{nf3}(\omega) = \frac{1}{2\pi^3}\left(\frac{e^2 P^{\uparrow}_{f}}{2E_f}\right)^2 \int d^3q \int d^3k \, \frac{\theta(E(\underline{p}-\underline{q})\downarrow - E_f - \phi)\,\theta((1-2\Delta)^{1/2} - k)}{((\underline{p}-\underline{q}-\underline{k})^2 + q^2_{fc})^2}$$

$$\times \theta(|\underline{q}+\underline{k}| - (1-2\Delta)^{1/2})\,\delta(\underline{p}\cdot\underline{q} - q^2/2 - \omega)\,\delta(\underline{q}\cdot\underline{k} + q^2/2 - \omega) \qquad (23)$$

$$R^{\downarrow}_{nf4}(\omega) = \frac{1}{2\pi^3}\left(\frac{e^2 P^{\uparrow}_{f}}{2E_f}\right)^2 \int d^3q \int d^3k \, \frac{\theta(E(\underline{p}-\underline{q})\downarrow - E_f - \phi)\,\theta((1-2\Delta)^{1/2} - k)}{(q^2 + q^2_{fc})((\underline{p}-\underline{q}-\underline{k})^2 + q^2_{fc})}$$

$$\times \theta(|\underline{q}+\underline{k}| - (1-2\Delta)^{1/2})\,\delta(\underline{p}\cdot\underline{q} - q^2/2 - \omega)\,\delta(\underline{q}\cdot\underline{k} + q^2/2 - \omega) \qquad (24)$$

The total non-flip transition rate for the incoming spin-down electron can be obtained by summing up the above contributions. Thus one obtains

$$R^{\downarrow}_{nf}(\omega) = R^{\downarrow}_{nf1}(\omega) + R^{\downarrow}_{nf2}(\omega) + R^{\downarrow}_{nf3}(\omega) + 2R^{\downarrow}_{nf4}(\omega) \qquad (25)$$

The factor 2 in the last term arises from the equal contributions from the diagrams Fig.7g and 7h representing the exchange process.

If the incoming electron is polarized to be a spin-up electron, then the possible non-flip processes are as shown in Fig.8. Again if we denote $R^{\uparrow}_{nf1}(\omega)$. $R^{\uparrow}_{nf2}(\omega)$, $R^{\uparrow}_{nf3}(\omega)$, and $R^{\uparrow}_{nf4}(\omega)$ for the non-flip transition rates associated with the diagrams Fig.8b, 8d, 8f and 8g and 8h, respectively, we can express the final expressions for these non-flip rates as follows:

$$R^{\uparrow}_{nf1}(\omega) = \frac{1}{2\pi^3}\left(\frac{e^2 P^{\uparrow}_f}{2E_f}\right)^2 \int d^3q \int d^3k \, \frac{\theta(E(\underline{p}-\underline{q})\uparrow - E_f - \phi)\,\theta((1-2\Delta)^{1/2}-k)}{(q^2+q^2_{fc})^2}$$

$$\times \theta(|\underline{q}+\underline{k}|-(1-2\Delta)^{1/2})\,\delta(\underline{p}\cdot\underline{q}-q^2/2-\omega)\,\delta(\underline{q}\cdot\underline{k}+q^2/2-\omega) \qquad (26)$$

$$R^{\uparrow}_{nf2}(\omega) = \frac{1}{2\pi^3}\left(\frac{e^2 P^{\uparrow}_f}{2E_f}\right)^2 \int d^3q \int d^3k \, \frac{\theta(E(\underline{p}-\underline{q})\uparrow - E_f - \phi)\,\theta(1-k)}{(q^2+q^2_{fc})^2}$$

$$\times \theta(|\underline{q}+\underline{k}|-1)\,\delta(\underline{p}\cdot\underline{q}-q^2/2-\omega)\,\delta(\underline{q}\cdot\underline{k}+q^2/2-\omega) \qquad (27)$$

$$R^{\uparrow}_{nf3}(\omega) = \frac{1}{2\pi^3}\left(\frac{e^2 P^{\uparrow}_f}{2E_f}\right)^2 \int d^3q \int d^3k \, \frac{\theta(E(\underline{p}-\underline{q})\uparrow - E_f - \phi)\,\theta(1-k)}{((\underline{p}-\underline{q}-\underline{k})^2+q^2_{fc})^2}$$

$$\times \theta(|\underline{q}+\underline{k}|-1)\,\delta(\underline{p}\cdot\underline{q}-q^2/2-\omega)\,\delta(\underline{q}\cdot\underline{k}+q^2/2-\omega) \qquad (28)$$

Recalling that Figs.8g and 8h contribute the same scattering amplitudes to the exchange process,

$$R^{\uparrow}_{nf4}(\omega) = \frac{1}{2\pi^3}\left(\frac{e^2 P^{\uparrow}_f}{2E_f}\right)^2 \int d^3q \int d^3k \, \frac{\theta(E(\underline{p}-\underline{q})\uparrow - E_f - \phi)\,\theta(1-k)}{(q^2+q^2_{fc})((\underline{p}-\underline{q}-\underline{k})^2+q^2_{fc})}$$

$$\times \theta(|\underline{q}+\underline{k}|-1)\,\delta(\underline{p}\cdot\underline{q}-q^2/2-\omega)\,\delta(\underline{q}\cdot\underline{k}+q^2/2-\omega) \qquad (29)$$

The total non-flip transition rate $R^{\uparrow}_{nf}(\omega)$ can then be obtained by summing up the above contributions

$$R^{\uparrow}_{nf}(\omega) = R^{\uparrow}_{nf1}(\omega) + R^{\uparrow}_{nf2}(\omega) + R^{\uparrow}_{nf3}(\omega) + 2R^{\uparrow}_{nf4}(\omega) \qquad (30)$$

IV. RESULTS AND DISCUSSIONS

The results of the present calculations are the four inelastic scattering rates: $R^{\uparrow}_{nf}$, $R^{\downarrow}_{nf}$, $R^{\uparrow}_{f}$ and $R^{\downarrow}_{f}$, for both Models A and B. Each transition rate is a function of the primary electron energy E_0, and of the energy loss ω (the momentum loss $\underline{q}$ being integrated over).

All values of the rates obtained from our model calculations are expressed in terms of a common factor $\frac{1}{2\pi^3}\left\{\frac{e^2 p^{\uparrow}_F}{2E_F}\right\}^2$.

From these four basic rates, we can also define other useful quantities:

The total energy loss rate for an unpolarized beam
$$= \tfrac{1}{2}\left(R^{\uparrow}_{nf} + R^{\downarrow}_{nf} + R^{\uparrow}_{f} + R^{\downarrow}_{f}\right)$$

The inelastic rate for creation of polarized electrons with energy $E_0 - \omega$ from an unpolarized beam (energy E_0)
$$= \begin{cases} \tfrac{1}{2}\left(R^{\uparrow}_{nf} + R^{\downarrow}_{f}\right) : \text{spin-up} \\ \tfrac{1}{2}\left(R^{\downarrow}_{nf} + R^{\uparrow}_{f}\right) : \text{spin-down} \end{cases}$$

The total loss rate (energy loss ω) of a spin-up (down) polarized beam
$$= R^{\uparrow(\downarrow)} = R^{\uparrow(\downarrow)}_{nf} + R^{\uparrow(\downarrow)}_{f}$$

hence we obtain

The relative spin asymmetry between total loss rates for a polarized incident beam
$$= A_{in}(E_0,\omega)$$
$$= \frac{\left(R^{\uparrow}_{nf} + R^{\uparrow}_{f}\right) - \left(R^{\downarrow}_{nf} + R^{\downarrow}_{f}\right)}{\left(R^{\uparrow}_{nf} + R^{\uparrow}_{f}\right) + \left(R^{\downarrow}_{nf} + R^{\downarrow}_{f}\right)}$$

The polarization of the inelastically scattered beam (energy $E_0-\omega$) for an unpolarized incident beam (energy E_0)
$$= A_{out}(E_0,\omega)$$
$$= \frac{\left(R^{\uparrow}_{nf} + R^{\downarrow}_{f}\right) - \left(R^{\downarrow}_{nf} + R^{\uparrow}_{f}\right)}{\left(R^{\uparrow}_{nf} + R^{\downarrow}_{f}\right) + \left(R^{\downarrow}_{nf} + R^{\uparrow}_{f}\right)}$$

We present our results both as a function of the energy loss ω for a fixed primary energy E_0, and as a function of E_0 for a fixed ω, The range of E_0 chosen goes up to 10 eV for Model A, and up to 200 eV for Model B. These energy ranges, we stress, are chosen because Model A is expected to retain meaning only for extremely low primary energies. Model B is valid for higher energies. However, it should be noted that in reality the distribution of outgoing electrons with kinetic energies $(E_0-\omega)$ lower than $\sim$30 eV is dominated by secondaries. These are created through a cascade of inelastic events and are not described here at all. Hence the

present single scattering results cannot be compared with experiment in this region.

Paramagnet: Figs.2 and 3 give the flip rate $R_f^{\uparrow}$ and non-flip $R_{nf}^{\uparrow}$ rate for a spin-up incoming electron interacting with a paramagnetic metal. Fig.2 gives the rate for varying energy loses ω at a fixed primary energy. We note that for $\omega > 60$ eV $R_f^{\uparrow} > R_{nf}^{\uparrow}$. Whilst from Fig.3, $R_f^{\uparrow}$ is much greater than $R_{nf}^{\uparrow}$ for most primary energies at the maximum ω. Obviously such effects can only be observed with the use of some form of spin analyzer. Nevertheless, it is interesting to see that there is a predominance of spin up (down) electrons (Fig.2) for $\omega > 60$ eV when using a spin polarized incident beam. A more thorough discussion of this and other aspects of spin-polarized spectroscopy of paramagnets is deferred to a later paper.

Ferromagnet; Model A

ω-dependence: Fig.9 shows the ω-dependent calculated rates for $E_0 = 5$ eV. We note several facts:

a) The non-flip rate is larger for down than for up-spin electrons;

b) The non-flip rates decrease for increasing energy loss;

c) The flip rate (here only $R_f^{\downarrow}$ is non-zero as there are no spin-down electrons in the ground state)is instead an increasing function;

d) The flip rate is generally negligible with respect to the non-flip rate (for low E_0) at small energy losses ω.

The following comments help to understand these results:

a) The non-flip rate for a down spin electron does not have an exchange contribution (see Fig.5), while that for an upspin has (see Fig.4, with the spins reversed). The exchange contribution is of opposite sign to the direct one, leading to $R_{nf}^{\downarrow} > R_{nf}^{\uparrow}$. Quantitatively this fact is well-recognized, and quite lucidly pointed out by Bringer et al. [9], as well as Rendell and Penn [17]. However we find the exchange cancellation of the spin-up inelastic non-flip rate much less dramatic than expected on the grounds of Feder's [8] and Bringer et al's. [9] crude assumption $R_{nf}^{\uparrow}/R_{nf}^{\downarrow} = n^{\downarrow}/n^{\uparrow}$. This last quantity equals zero in Model A, while the left-hand side is typically of the order of 0.5 for Model A.

b) The non-flip rates basically involve energy-loss functions of the type $\mathrm{Im}\,\epsilon^{-1}(q,\omega)$ [17], a quantity which (after the plasmon peak, here absent) is generally decreasing for large ω. This accounts for the decreasing behaviour of $R_{nf}(\omega)$.

c) The most probable spin-flip event occurs when $\omega \sim E_0$ since in that case the intermediate energy $\epsilon+\omega$ is also $\sim E_0$, and in effect the primary electron need only lose a minimum between ϕ and $\phi + E_f$, small in comparison with E_0.

d) In spite of this contrasting behaviour of R_{nf} and R_f, the flip rate remains well below the non-flip rate except perhaps for the largest energy loss $\omega = E_0$, for small E_0.

We have also tried to judge the extent to which the present conclusions are influenced by the particular crude choice of screened Coulomb interaction (see Eq.(3)), by re-doing the same calculation with an unscreened Coulomb interaction $V(q) = 4\pi e^2/q^2$. The result, shown in Fig.9, indicates that all of the above conclusions remain true in that case, suggesting that, while numerical values would of course dependend substantially on the choice of V, the physical conclusions in the end do not.

E_0-dependence: We have chosen two ways of presenting our results for the primary electron energy dependence. The first is for fixed energy loss ω, as exemplified in Fig.10. The second is for $\omega = E_0$, shown in Fig.11. This latter choice is suggested by the fact that it is in this condition that spin-flip appears the most probable, (although in practice for high ω the single scattering event would be swamped by secondary events).

Examination of these results leads to the following conclusions:

a) At fixed energy loss ω, both non-flip rates tend to constant values whilst the flip rate rapidly decreases for increasing E.

b) For maximum loss, i.e. $\omega = E_0$, the E_0-dependence is more interesting. While at low E_0 ($\lesssim E_F$) the flip rate has no weight, it does pick up and remain about constant for larger energies, while at the same time the non-flip rates drop. Remarkably, for $E_0 \gtrsim 8$ eV, only up spins seem to survive. Unfortunately, however, the model is inapplicable in this energy range so that it is doubtful whether the prediction that the very low energy inelastically scattered electrons should be up-spin polarized, which Model A makes, has actually anything to do with real situations, like that of Fe.

Asymmetry parameters: Lastly, we consider the asymmetry parameters A_{in} and A_{out}, defined previously. Fig.12 shows the behaviour obtained from the rates of Fig.11, for Model A. The predicted low-energy asymmetries are large, in the order of 40% and larger. Interestingly enough, the asymmetry for an incoming polarized beam A_{in} is found to stay negative since the inelastic rate is larger for spin-down electrons. This is to be contrasted with the asymmetry for an incoming unpolarized beam, A_{out}, which changes sign from negative to positive, as E_0 increases from 1 eV to 5 eV. Thus an outgoing beam of nearly-zero energy inelastic electrons ($\omega \sim E_0$) should switch from initially up-spin-polarized to down-spin-polarized, when E_0 is increased. This behaviour is to be attributed to the sharp onset of spin-flip transitions as shown in Fig.11.

Model B

ω-depedence: The four transition rates for Model B are displayed in Fig.13. The following features are evident:

a) The qualitative behaviour is similar to that already found for Model A, in particular the flip amplitudes show a monotonic increase with energy loss ω;

b) Of the two flip rates, $R_f^{\downarrow}$ is larger than $R_f^{\uparrow}$ (in Model A $R_f^{\uparrow}$ was zero);

c) The non-flip amplitudes exhibit three qualitatively different regimes: an increase up to $\omega \sim E_F$ followed by a drop and finally by a further increase between ~ 60 eV and E_0;

d) The down and up-spin non-flip rates are very close to one another. At low $\omega (< E_0/2)$ $R_{nf}^{\downarrow} > R_{nf}^{\uparrow}$ and at $\omega > E_0/2$ the reverse is found. However, the total rate $R_{nf}^{\downarrow} + R_f^{\downarrow}$ is always found to be larger than $R_{nf}^{\uparrow} + R_f^{\uparrow}$ for an incoming polarized beam.

While for point a) the same comments apply as for Model A, the remaining findings require some extra comments:

b) The spin flip inelastic rate is larger for down-spin electrons, because it involves exciting an up electron, and there are more of those;

c) The low-energy peak of R_{nf} can be ascribed to exhaustion of the f-sum rule in the energy range between E_F and ω_p. Of course, proper inclusion of dynamical screening effects would have produced a better-looking plasmon peak, but the essence is the same. As for the nature of the increase near $\omega = E_0$, we notice that it is due to one of the four separate diagrams that contribute to R_{nf}. As explained in Sec.III

these four terms are R_{nf1}, R_{nf2}, R_{nf3} and R_{nf4} (see Fig.14). The process R_{nf3} is the one that increases with ω and becomes dominant near $\omega = E_0$. It should be stressed again, however, that this part of the spectrum is not to be taken seriously, because the processes that generate secondary electron cascades (i.e. a more realistic model) have not been included in the calculation.

d) The change of sign of $R_{nf}^{\uparrow} - R_{nf}^{\downarrow}$ from negative to positive as the primary energy is increased can be understood by splitting the non-flip rates into its four contributions as shown in Fig.14. Of those, $R_{nf1}^{\downarrow} + R_{nf2}^{\downarrow} - 2R_{nf4}^{\downarrow}$ is always larger than the corresponding term for spin-down electron. This is intuitively clear from the simple fact that $n^{\uparrow} > n^{\downarrow}$. However, for the process $R_{nf3}^{\downarrow}$ the opposite is true, and since this term rapidly increases with increasing ω, this leads to a reversal of behaviour for $\omega > E_0/2$.

E_0-dependence: Fig.15 shows the primary energy dependence of the loss rates for a fixed energy loss $\omega = 60$ eV. Examination of the results leads to the following comments:

a) For a fixed energy loss ω, the spin-flip rate R_F is roughly comparable to the non-flip rate near $\omega = E_0$ and it drops as E_0 increases;

b) The separate terms contributing to total non-flip rate are plotted in Fig.16. R_{nf1} and R_{nf2} drop slowly whereas R_{nf3} and $(-2R_{nf4})$ drop quite quickly with increasing E_0. At low energies the R_{nf3} and $(-2R_{nf4})$ terms are dominant and at higher energies R_{nf1} and R_{nf2} become dominant;

c) The spin-flip rate $R_f^{\downarrow}$ for a spin-down electron is always larger than that for a spin-up electron at all energies;

d) For low energies, $(60 < E_0 \lesssim 80$ eV), the non-flip rate $R_{nf}^{\uparrow}$ is larger than $R_{nf}^{\downarrow}$ and the situation becomes reversed at higher energies. However, the difference between non-flip and flip rates for spin-up and spin-down, respectively, are compatible to each other so that rate $R^{\downarrow}$ is found to be larger than $R^{\uparrow}$ at all energies for an incoming polarized beam.

Fig.17 illustrates the behaviour expected when varying the primary electron energy, and measuring $\omega = E_0$. As with Model A, the flip and non-flip rates rapidly approach one another for large E_0. We stress again that this behaviour will probably be impossible to observe, due to the presence of secondaries.

Asymmetry parameters: Figs.18 and 19 show the behaviour of the asymmetry parameters for Model B. These parameters are extracted from the rates of Figs.13 and 15, respectively. A third asymmetry parameter A_{nf} is introduced; $A_{nf} = (R^{\uparrow}_{nf} - R^{\downarrow}_{nf})/(R^{\uparrow}_{nf} + R^{\downarrow}_{nf})$, which appears to be more appropriate for the purpose of making contact with the calculation of Rendell and Penn [17], who do not consider explicitly spin-flip processes. The predicted low-energy loss asymmetry parameters are rather small (as compared to those in Model A) of the order of 1%. Here again, the asymmetry for incoming polarized beam A_{in} is found to stay negative as in Model A. Apart from the scaling factor the behaviour of all quantities in Model B of Fig.18 are roughly similar to those of Model A in Fig.12 and therefore similar comments apply.

Fig.19 requires some extra comments. The asymmetry for an incoming unpolarized beam, A_{out}, changes sign from positive to negative, as E_0 increases from 60 eV to 200 eV for a fixed energy loss ω = 60 eV. Thus an outgoing beam suffering fixed energy loss should switch from initially up-polarized to down-polarized, when E_0 is increased.

We wish also to point out that the present results for Model B qualitatively support the assumption of Bringer et al. [9], that $\lambda^{\uparrow}/\lambda^{\downarrow} = R^{\uparrow}/R^{\downarrow} = n^{\uparrow}/n^{\downarrow}$ where λ represents the mean-free-path which is inversely proportional to the loss rate. However, we find that quantitaively this assumption overestimates the exchange effects. For fixed electron energy E_0 = 100 eV we find that $R^{\downarrow}/R^{\uparrow}$ is between 1.04 and 1.18 and for fixed energy loss ω = 60 eV, it lies between 1.08 and 1.12, the assumed value of $n^{\uparrow}/n^{\downarrow}$ for Δ = 1.5 eV, is 1.22. Therefore the effects of exchange are weaker than supposed by Bringer et al. [9]. On the other hand, our results demonstrate that proper inclusion of spin-flip exchange processes is able to reverse Rendell and Penn's [17] original conclusion that the inelastic mean free path E_0 (in for example Fe), is shorter for up spins than for down spins. Our own work [6] based on the general approach presented here shows that in fact the opposite is true in agreement with experimental findings [3,4].

ACKNOWLEDGMENTS

Two of the authors (C.J.B and S.Y.) would like to thank Professor Abdus Salam, the International Atomic Enegy Agency and UNESCO for hospitality at the International Centre for Theoretical Physics. Trieste. One of the authors (C.J.B.) gratefully acknowledges the Royal Society (London) for an overseas fellowship.

APPENDIX

The integrals derived in the text contain one of the theta-delta ($\theta\delta$) products given in Table A1. These products define the regions of ω, $\underline{q}$ and $\underline{k}$ space where the integrals have a non-zero value. The table gives the $\theta\delta$-product for each integral considered and the corresponding figure which determines the $|\underline{k}|$ and $|\underline{q}|$ limits on the integrals. Fig. A1 gives the Stoner continuum. For all integrals there are essentially three integrands, these are given in Table A2. We begin by considering the following generalized integral:

$$\int d^3q \int d^3k \; \frac{\theta(|\underline{q}+\underline{k}|-S_1)\,\theta(S_2-|\underline{k}|)}{Pkq^2\,((\underline{p}-\underline{q}-\underline{k})^2+q_{fe}^2)^2} \times \delta\left\{\mu_{\underline{p}\,\underline{q}} - \frac{f\omega\Delta q}{Pq}\right\}\delta\left\{\mu_{\underline{k}\,\underline{q}} - \frac{g\omega\Delta q}{kq}\right\} \qquad (I)$$

where

$$\mu_{\underline{a}\,\underline{b}} = \hat{\underline{a}}\cdot\hat{\underline{b}} = \cos\theta_{ab}$$

From Table A1, $f_{\omega,\Delta,q}$ may have the following forms: $\omega-\Delta-\frac{q^2}{2}$, $\omega+\Delta-\frac{q^2}{2}$, $\omega-\frac{q^2}{2}$ and $g_{\omega\Delta q}$: $\omega-\Delta+\frac{q^2}{2}$, $\omega+\Delta+\frac{q^2}{2}$ and $\omega+\frac{q^2}{2}$. The θ functions require that the magnitude of the vector $\underline{q}+\underline{k}$ be greater than the radius S_1 of a sphere and similarly for the vector $\underline{k}$ to have its magnitude less than S_2. Expanding the denominator we have:

$$((\underline{p}-\underline{q}-\underline{k})^2+q_{fe}^2)^{-2} = (p^2+q^2+k^2-2pq\mu_{\underline{p}\,\underline{q}}-2pk\mu_{\underline{p}\,\underline{k}}+2qk\mu_{\underline{q}\,\underline{k}}+q_{fe}^2)^{-2}$$

in order to utilize the delta functions we write $\mu_{\underline{p}\underline{k}}$ as follows:

$$\mu_{\underline{p}\underline{k}} = \mu_{\underline{p}\underline{q}}\,\mu_{\underline{k}\underline{q}} + \left(1-\mu^2_{\underline{p}\underline{q}}\right)^{1/2}\left(1-\mu^2_{\underline{k}\underline{q}}\right)^{1/2}\cos\Phi \qquad \text{(II)}$$

where Φ is given in Fig. A6 and is the angle between the planes containing $(\underline{q},\underline{k})$ and $(\underline{p},\underline{q})$ measured perpendicular to $\underline{q}$. With the above choice of angles the 6-dimensional integral becomes,

$$\int d^3q \int d^3k \longrightarrow 2\pi \int_{q_m}^{q_x} q^2 dq \int_{-1}^{1} d\mu_{\underline{p}\underline{q}} \int_{k_m}^{k_x} k^2\,dk \int_{-1}^{1} d\mu_{\underline{q}\underline{k}} \int_0^{2\pi} d\Phi$$

The limits q_x, q_m, k_x and k_m are determined by geometrical analysis of the θ and δ-functions [13]. For a given integral a definite region in q,ω space is defined by the $\theta\delta$-products. These regions are given in Figs. A1 to A5. Carrying out the Φ, $\mu_{\underline{q}\underline{k}}$ and $\mu_{\underline{p}\underline{k}}$ integrations gives:

$$\frac{4\pi^2}{P}\int_{q_m}^{q_x} dq \int_{k_m}^{k_x} dk\, \frac{k\,C}{(C^2-D)^{3/2}} \qquad \text{(III)}$$

with

$$C = p^2 + q^2 + k^2 - 2f_{\omega\Delta q} + 2g_{\omega\Delta q} - \frac{2}{q^2} f_{\omega\Delta q}\, g_{\omega\Delta q} + q^2_{ft}$$

$$D = 4p^2k^2\left\{1 - \frac{f^2_{\omega\Delta q}}{(Pq)^2}\right\}\left\{1 - \frac{g^2_{\omega\Delta q}}{(kq)^2}\right\} \qquad \text{(IV)}$$

k-integration is now straightforward and yields

$$\frac{4\pi^2}{P}\int_{q_m}^{q_x} dq \left\{\frac{(2\alpha-\mu)k + \mu\alpha - 2\nu}{(4\nu-\mu^2)(k^2+\mu k+\nu)^{1/2}}\right|_{k^2_m}^{k^2_x}\Bigg\} \qquad \text{(V)}$$

with

$$\mu = [2\alpha - \beta]$$

$$\nu = [\alpha^2 + \gamma]$$

$$\alpha = C - k^2$$

$$\beta = D \Big/ \left\{k^2 - \frac{g^2_{\omega\Delta q}}{q^2}\right\}$$

$$\gamma = \beta\, g^2_{\omega\Delta q} / q^2 \qquad \text{(VI)}$$

finally the q-integral is done numerically by gaussian quadrature.

For the integral

$$\int d^3q \int d^3k\, \frac{\theta(|\underline{q}+\underline{k}| - S_1)\,\theta(S_2 - |\underline{k}|)}{Pkq^2(q^2+q^2_{ft})((\underline{p}-\underline{q}-\underline{k})^2 + q^2_{ft})}$$

$$\times \left\{\mu_{pq} - \frac{f_{\omega\Delta q}}{Pq}\right\}\left\{\mu_{kq} - \frac{g_{\omega\Delta q}}{kq}\right\} \qquad \text{(VII)}$$

similar analysis leads to

$$\frac{4\pi}{P}\int_{q_m}^{q_x} dq \left\{ \frac{1}{(q^2+q_{fe}^2)} \int_{k_m}^{k_x} \frac{k\,dk}{(C^2-D)^{1/2}} \right\} \qquad \text{(VIII)}$$

with C and D defined above. Completing the k-integration we are left with

$$\frac{4\pi^2}{P}\int_{q_m}^{q_x} dq \frac{1}{(q^2+q_{fe}^2)} \ln\sqrt{\frac{2(k_x^4+\mu k_x^2+\nu)^{1/2}+2k_x^2+\mu}{2(k_m^4+\mu k_m^2+\nu)^{1/2}+2k_m^2+\mu}} \qquad \text{(IX)}$$

with ν and μ as above. As before the q-integral is done numerically by gaussian quadrature.

REFERENCES

1) Kirschner, J., "Polarized electrons at surfaces", Springer Tracts in Modern Physics, Vol.106 (Springer-Verlag, Heidelberg 1985).

2) Feder, R., in Polarized Electrons in Surface Physics, Ed. R. Feder (World Scientific Publishing Co., Singapore, 1985), p.125; Siegmann, H.C., Meier, E., Erbudak, M. and Landolt, M., Adv. Electron Electron Phys. 62, 1 (1984).

3) Hopster, H., Raue, R. and Clauberg, R., Phys. Rev. Lett. 53, 695 (1984).

4) Kirschner, J., Rebenstorff, D. and Ibach, H., Phys. Rev. Lett. 53, 698 (1984).

5) Yin, S. and Tosatti, E., ICTP, Trieste, preprint IC/81/129.

6) Glazer, J. and Tosatti, E., Solid State Commun. 52, 905 (1984).

7) Campagna, M., Meier, F., Pierce, D.T., Sattler, K. and Siegmann, H.C., in Handbook of Surfaces and Interfaces, Ed. L. Dobrzynski (Garland STPM Press, New York, 1978), Vol.I.

8) Feder, R., Solid State Commun. 31, 821 (1979).

9) Bringer, A., Campagna, M., Feder, R., Gudat, W., Kisker, E. and Kahlman, K., Phys. Rev. Lett. 42, 1705 (1979).

10) Froitzheim, H.,"Electron energy loss spectroscopy" in Electron Spectroscopy for Surface Analysis, Topics in Current Physics, Ed. H. Ibach (Springer Verlag, Heidelberg, 1977), Vol.4.

11) Helman, J.S. and Baltensperger, W., Phys. Rev. B22, 1300 (1980).

12) Siegmann, H.C., Pierce, D.T. and Celotta, R.J., Phys. Rev. Lett. 46, 452 (1981).

13) Fetter, A.L. and Walecka, J.D., Quantum Theory of Many Particle Systems (McGraw Hill, New York 1971); Pines, D., The Many-Body Problem, a Lecture Note and Reprint Volume (Benjamin, New York 1962).

14) Callaway, J. and Wang, C.S., Phys. Rev. B16, 2095 (1977).

15) Colavita, E., De Crescenzi, M., Papagno, L., Scarmozzino, R., Caputi, L.S., Rosei, R. and Tosatti, E., Phys. Rev. B25, 2490 (1982).

16) Sickafus, E.N., Phys. Rev. B16, 1448 (1977).

17) Rendell, R.W. and Penn, D.R., Phys. Rev. Lett. 45, 2057 (1980).

TABLE A1

$\theta\delta$-product	Eq. number of integral	ω-q figure number
$\theta(\lvert q+k\rvert - \sqrt{1-2\Delta})\theta(1-k)\delta(\omega-\Delta - \frac{q^2}{2} - \underline{k}\cdot\underline{q})\delta(\omega-\Delta + \frac{q^2}{2} - p\cdot q)$	19	A1
$\theta(\lvert q+k\rvert-1)\theta(\sqrt{1-2\Delta} - k)\delta(\omega+\Delta - \frac{q^2}{2} - \underline{k}\cdot\underline{q})\delta(\omega+\Delta + \frac{q^2}{2} - p\cdot q)$	21	A2
$\theta(\lvert q+k\rvert - \sqrt{1-2\Delta})\theta(\sqrt{1-2\Delta} - k)\delta(\omega - \frac{q^2}{2} - \underline{k}\cdot\underline{q})\,\delta(\omega + \frac{q^2}{2} - p\cdot q)$	22,24	A3
	25,27	
$\theta(\lvert q+k\rvert-1)\theta(1-k)\delta(\omega - \frac{q^2}{2} - \underline{k}\cdot\underline{q})\delta(\omega + \frac{q^2}{2} - \underline{p}\cdot\underline{q})$	6,7,8,9,17, 23,28,29,30	A4
$\theta(K(q+k)+-\Delta)\theta(1-k)\delta(\omega-\Delta + \frac{q^2}{2} - \underline{p}\cdot\underline{q})\delta(\omega-\Delta - \frac{q^2}{2} - \underline{q}\cdot\underline{k})$	14	A5

TABLE A2

Integrand	Contained in Eqs.
$((\underline{p}-\underline{q}-\underline{k})^2 + \bar{q}_{ft}^2)^{-2}$	6,8,14,19,21, 24,29
$(q^2 + \bar{q}_{ft}^2)^{-1}((\underline{p}-\underline{q}-\underline{k})^2 + \bar{q}_{ft}^2)^{-1}$	9,25, 30
$(q^2 + \bar{q}_{ft}^2)^{-2}$	7,17,22,23, 27,28

FIGURE CAPTIONS

Fig. 1 a) A possible spin-flip process for an incoming spin-down electron in a paramagnetic metal. Here the circled cross ⊗ indicates the detection process.
b) A Feynman diagram representing the spin-flip process.

Fig. 2 Comparison of $R_f^{\downarrow}(E_0,\omega)$ and $R_{nf}^{\downarrow}(E_0,\omega)$ for a paramagnetic metal at fixed primary energy E_0 = 100 eV and varying energy loss ω. Values of R are units of $\frac{1}{2\pi^3}\left(\frac{e^2 p_F^{\uparrow}}{2E_F}\right)^2$ and E_F = 11.1 eV, Δ=0, ϕ = 4.3 eV, $q_{FT}/p_F^{\uparrow}$ = 1.1887. Note that for a paramagnetic metal $R_{f(nf)}^{\downarrow} = R_{f(nf)}^{\uparrow}$.

Fig. 3 Comparison of $R_f^{\downarrow}(E_0,\omega)$ and $R_{nf}^{\downarrow}(E_0,\omega)$ for a paramagnetic metal, calculated at $\omega = E_0$, as a function of kinetic energy E_0 above the vacuum level. Other parameters as in Fig. 2.

Fig. 4 Possible non-flip processes and the corresponding Feynman diagrams for an incoming spin-down electron in a paramagnetic metal. The circled crosses ⊗ indicate the detection processes and the dashed line the vacuum level. Note that the pairs of diagrams (b) and (b'), and (e) and (f) contribute equally to their respective processes.

Fig. 5 (a) and (b): The spin-flip process and
(c) and (d): non-flip process for an incoming electron with spin antiparallel to the majority spin electrons in Model A.

Fig. 6 (a) and (b): The spin-flip process for an incoming electron with spin anti-parallel to the majority spin electrons and
(c) and (d): the spin-flip process for an incoming electron with spin parallel to the majority spin electrons in Model B.

Fig. 7 The non-flip processes that are possible for an incoming electron with spin antiparallel to the majority spin electrons in Model B.

Fig. 8 The non-flip processes that are possible for an incoming electron with spin parallel to the majority spin electrons in Model B.

Fig. 9 Comparison of $R_f^{\downarrow}(E_0,\omega)$, $R_{nf}^{\downarrow}(E_0,\omega)$ and $R_{nf}^{\uparrow}(E_0,\omega)$ for Model A; with a statically screened potential (solid line) and an unscreened potential (dashed line), calculated at a fixed primary energy E_0 = 5 eV, as a function of energy loss ω E_f = 1.0 eV, Δ = 2.0 eV, ϕ = 4.3 eV, $q_{FT}/p_f^{\uparrow}$ = 0.924.

Fig. 10 Comparison of $R_f^{\downarrow}(E_0,\omega)$, $R_{nf}^{\downarrow}(E_0,\omega)$ and $R_{nf}^{\uparrow}(E_0,\omega)$ for Model A, calculated at fixed energy loss ω = 4.0 eV, as a function of primary energy E_0 above the vacuum level. $E_{0,min}$ denotes the minimum primary energy required for the observation of energy-loss processes. Other parameters as in Fig. 9.

Fig. 11 As Fig. 10 except $\omega = E_0$.

Fig. 12 Comparison of A_{out} and A_{in} using the data given in Fig. 11.

Fig. 13 Comparison of $R_f^{\downarrow(\uparrow)}(E_0,\omega)$ and $R_{nf}^{\downarrow(\uparrow)}(E_0,\omega)$ calculated at E_0 = 100 eV for Model B, as a function of energy loss ω. E_f = 11.93 eV, Δ = 1.5 eV, ϕ = 4.3 eV, $q_{FT}/p_F^{\uparrow}$ = 1.1467.

Fig. 14 a) Comparison of the separate contributions to the total non-flip rate $R_{nf}^{\downarrow}$ given for Model B in Fig. 13. The curves are related as follows (a) to $-2R_{nf4}^{\downarrow}$, (b) to $R_{nf1}^{\downarrow}$, (c) to $R_{nf2}^{\downarrow}$ and (d) to $R_{nf3}^{\downarrow}$.
b) As Fig. 14(a) but for $R_{nf}^{\uparrow}$.

Fig. 15 Comparison of $R_f^{\downarrow(\uparrow)}(E_0,\omega)$ and $R_{nf}^{\downarrow(\uparrow)}(E_0,\omega)$ calculated at ω = 60 eV for Model B as a function of primary energy E_0. Parameters as Fig. 13.

Fig. 16 a) Comparison of the separate contributions to the total non-flip rate $R_{nf}^{\downarrow}$ given for Model B in Fig. 15. The curves are related as follows, (a) to $-2R_{nf4}^{\downarrow}$, (b) to $R_{nf1}^{\downarrow}$, (c) to $R_{nf2}^{\downarrow}$ and (d) to $R_{nf3}^{\downarrow}$.
b) As Fig. 16(a) but for $R_{nf}^{\uparrow}$.

Fig. 17 Comparison of $R_f^{\downarrow(\uparrow)}(E_0,\omega)$ and $R_{nf}^{\downarrow(\uparrow)}(E_0,\omega)$ calculated at $\omega = E_0$, as a function of primary energy for Model B. Parameters as in Fig. 13.

Fig. 18 The spin asymmetry quantities A_{out} A_{in} and A_{nf} calculated using the data given in Fig. 13 for Model B.

Fig. 19 As Fig. 18 except data obtained from Fig. 15.

Fig. A1 The region in ω,q space for which integrals (I) and (VII) are non-zero, when defined by a $\theta\delta$-product with the following structure in dimensionless units (see text);
$\theta(|q+k| - \sqrt{1-2\Delta})\theta(1-k)\delta(\omega-\Delta - \frac{q^2}{2} - k\,q)\delta(\omega-\Delta + \frac{q^2}{2} - p\,q)$.
The curves are related as follows:
(a) $\Delta + \frac{q^2}{2} + q$, (b) $\Delta + \frac{q^2}{2} - q$, (c) $\Delta + q\sqrt{1-2\Delta} - \frac{q^2}{2}$,
(d) $\Delta - q\sqrt{1-2\Delta} - \frac{q^2}{2}$, (e) $\Delta - \frac{q^2}{2} - pq$ and (f) $\Delta - \frac{q^2}{2} + pq$.
E_x defines the maximum energy loss and for this case is equal to $E(p)\uparrow - E_f = \Delta + \frac{p^2}{2} - \frac{1}{2}$. $q_1 = 1 - \sqrt{1-2\Delta}$ and $q_2 = 1 + \sqrt{1-2\Delta}$.
The k-limits for integrals (III) and (VIII) depend on the values of q and ω. In region 1 : $k_m = |\frac{\omega-\Delta}{q} - \frac{q}{2}|$, $k_x = 1$, in region 2: $k_m = \sqrt{1-2\omega}$, $k_x = 1$; otherwise the integrals are zero.

Fig. A2 The same considerations as for Fig. A1 apply with a $\theta\delta$ product of the form: $\theta(|q+k|-1)\,\theta(\sqrt{1-2\Delta}-k)\delta(\omega+\Delta - \frac{q^2}{2} - k\cdot q)\delta(\omega+\Delta + \frac{q^2}{2} - p\cdot q)$
(a) $\frac{q^2}{2} + q\sqrt{1-2\Delta}-\Delta$, (b) $\frac{q^2}{2} - q\sqrt{1-2\Delta}-\Delta$, (c) $q - \frac{q^2}{2} - \Delta$ and
(d) $pq - \frac{q^2}{2} - \Delta$. $E_x = E(p)\uparrow - E_f = \frac{p^2}{2} - \frac{1}{2}$, $q_1 = 1 - \sqrt{1-2\Delta}$,
$q_2 = 1 + \sqrt{1-2\Delta}$.
In region 1: $k_m = |\frac{\omega+\Delta}{q} - \frac{q}{2}|$, $k_x = \sqrt{1-2\Delta}$;
In region 2: $k_m = \sqrt{1-2(\omega+\Delta)}$ $k_x = \sqrt{1-2\Delta}$, otherwise integrals zero.
(Note a rotation of π about the q axis will give the continuation of Fig. A1 for $\omega < 0$ for solid curves).

Fig. A3 The same considerations as for Fig. A1 with a $\theta\delta$-product of the form
$\theta(|q+k| - \sqrt{1-2\Delta})\theta(\sqrt{1-2\Delta}-k)\theta(\omega - \frac{q^2}{2} - k\cdot q)\delta(\omega+ \frac{q^2}{2} - p\cdot q)$
(a) $\frac{q^2}{2} + q\sqrt{1-2\Delta}$, (b) $\frac{q^2}{2} - q\sqrt{1-2\Delta}$, (c) $q\sqrt{1-2\Delta} - \frac{q^2}{2}$ and
(d) $pq - \frac{q^2}{2}$. $E_x = \Delta + \frac{p^2}{2} - \frac{1}{2} = E(p)\uparrow - E_F$. $q_1 = 2\sqrt{1-2\Delta}$.
In region 1: $k_m = |\frac{\omega}{q} - \frac{q}{2}|$, $k_x = \sqrt{1-2\Delta}$; in region 2: $k_m = \sqrt{1-2(\omega+\Delta)}$, $k_x = \sqrt{1-2\Delta}$; otherwise integrals are zero.

Fig. A4 $\theta\delta$-product of the form
$\theta(|q+k|-1)\theta(1-k)\delta(\omega - \frac{q^2}{2} - k\cdot q)\delta(\omega + \frac{q^2}{2} - p\cdot q)$.
(a) $\frac{q^2}{2} + q$, (b) $\frac{q^2}{2} - q$, (c) $q - \frac{q^2}{2}$, and (d) $pq - \frac{q^2}{2}$
$E_x = E(p)\uparrow - E_f = \frac{p^2}{2} - \frac{1}{2}$ $q_1 = 2$. In region 1: $k_m = |\frac{\omega}{q} - \frac{q}{2}|$,
$k_x = 1$; In region 2: $k_m = \sqrt{1-2\omega}$ $k_x = 1$; otherwise integral zero.

Fig. A5 $\theta\delta$-product of the form
$\theta(E(q+k)\uparrow-\Delta)\theta(1-k)\delta(\omega-\Delta + \frac{q^2}{2} - p\cdot q)\delta(\omega-\Delta - \frac{q^2}{2} - q\cdot k)$
(a) $\Delta + \frac{q^2}{2} + q$, (b) $\Delta + \frac{q^2}{2} - q$, (c) $\Delta - \frac{q^2}{2} + pq$ and
(d) $\Delta - \frac{q^2}{2} - pq$. $E_x = E(p)\uparrow - E_f = \Delta + \frac{p^2}{2} - \frac{1}{2}$.
In region 1: $k_m = |\frac{\omega-\Delta}{q} - \frac{q}{2}|$, $k_x = 1$, otherwise integral zero.

Fig. A6 Definition of Φ and angles used in the derivation of Eq. (II)

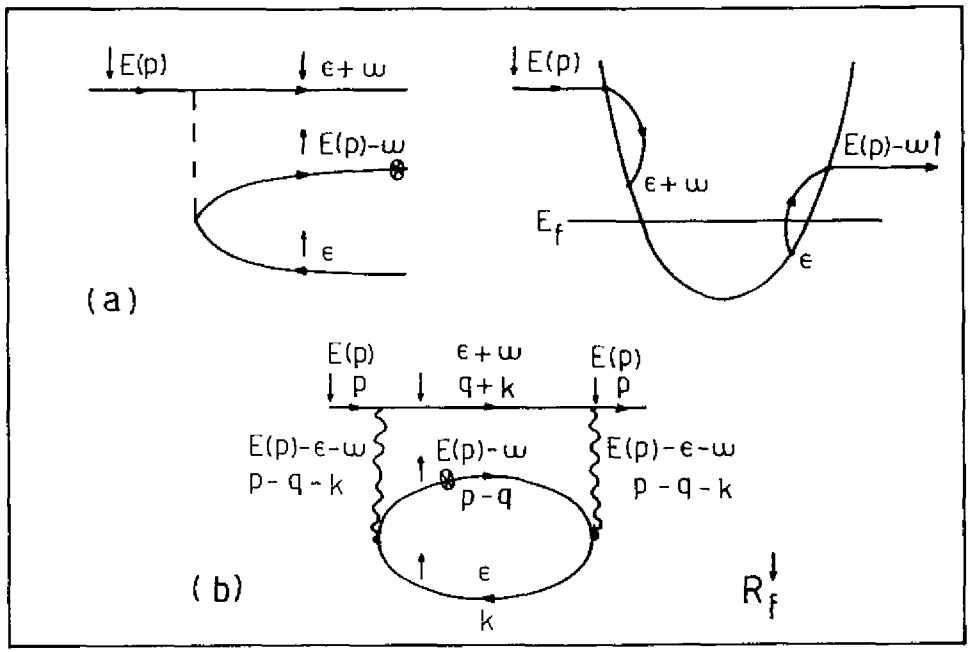
E(p)
ϵ+ω
E(p)-ω
ϵ
(a)
E(p)
E(p)-ω
ϵ+ω
E_f
ϵ
E(p)
ϵ+ω
E(p)
p
q+k
p
E(p)-ϵ-ω
p-q-k
E(p)-ω
p-q
E(p)-ϵ-ω
p-q-k
ϵ
(b)
k
R_f^↓

FIG. 1

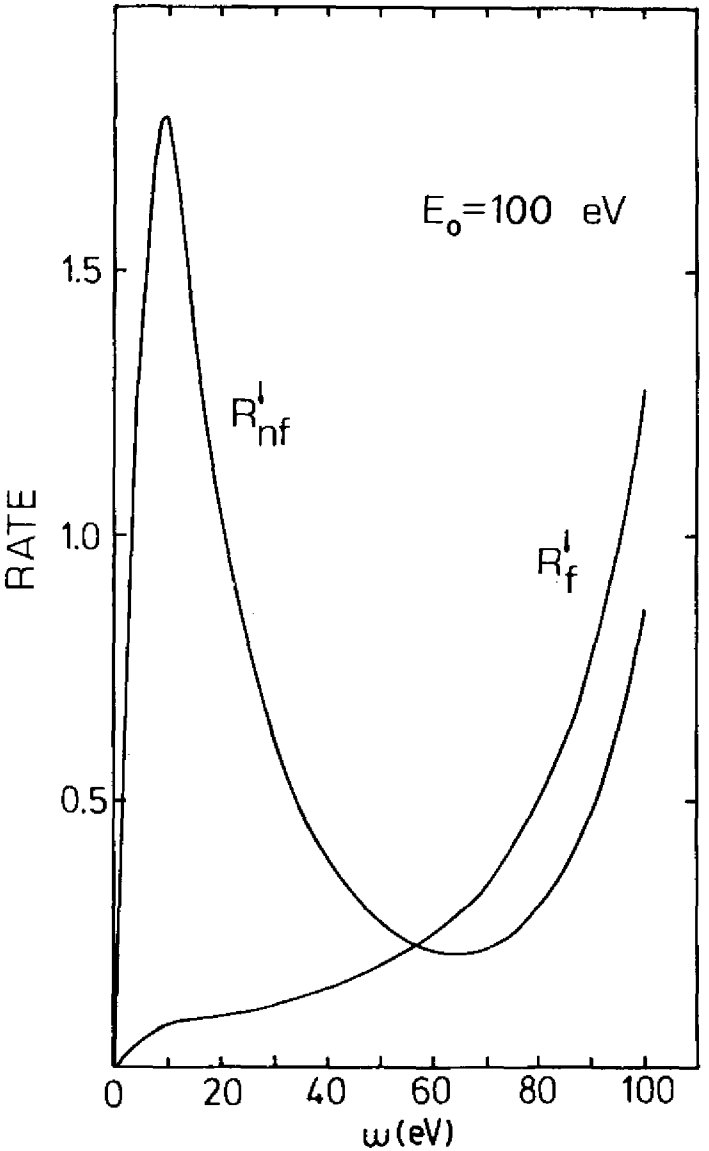
E_o=100 eV
RATE
1.5
1.0
0.5
R_nf^↓
R_f^↓
0
20
40
60
80
100
ω(eV)

FIG. 2

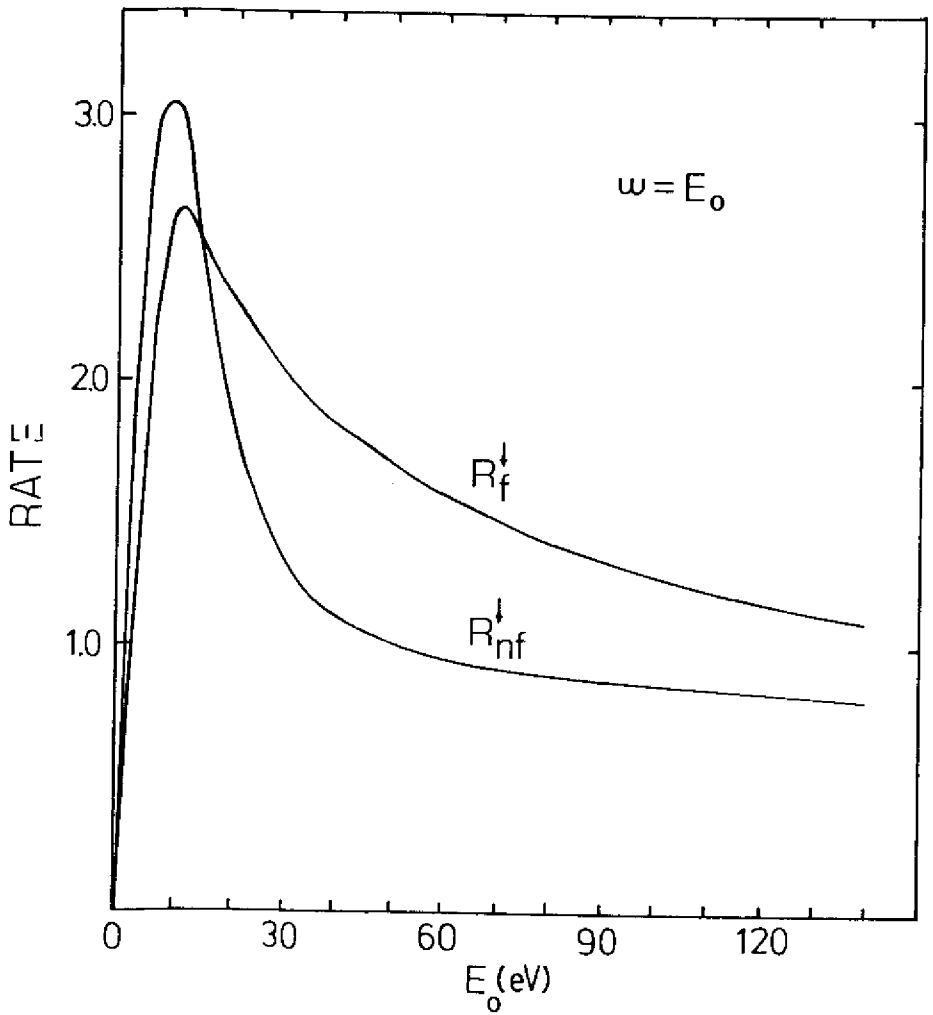
RATE
3.0
2.0
1.0
0
30
60
90
120
E_o(eV)
$\omega = E_o$
$R^{\downarrow}_f$
$R^{\downarrow}_{nf}$

FIG. 3

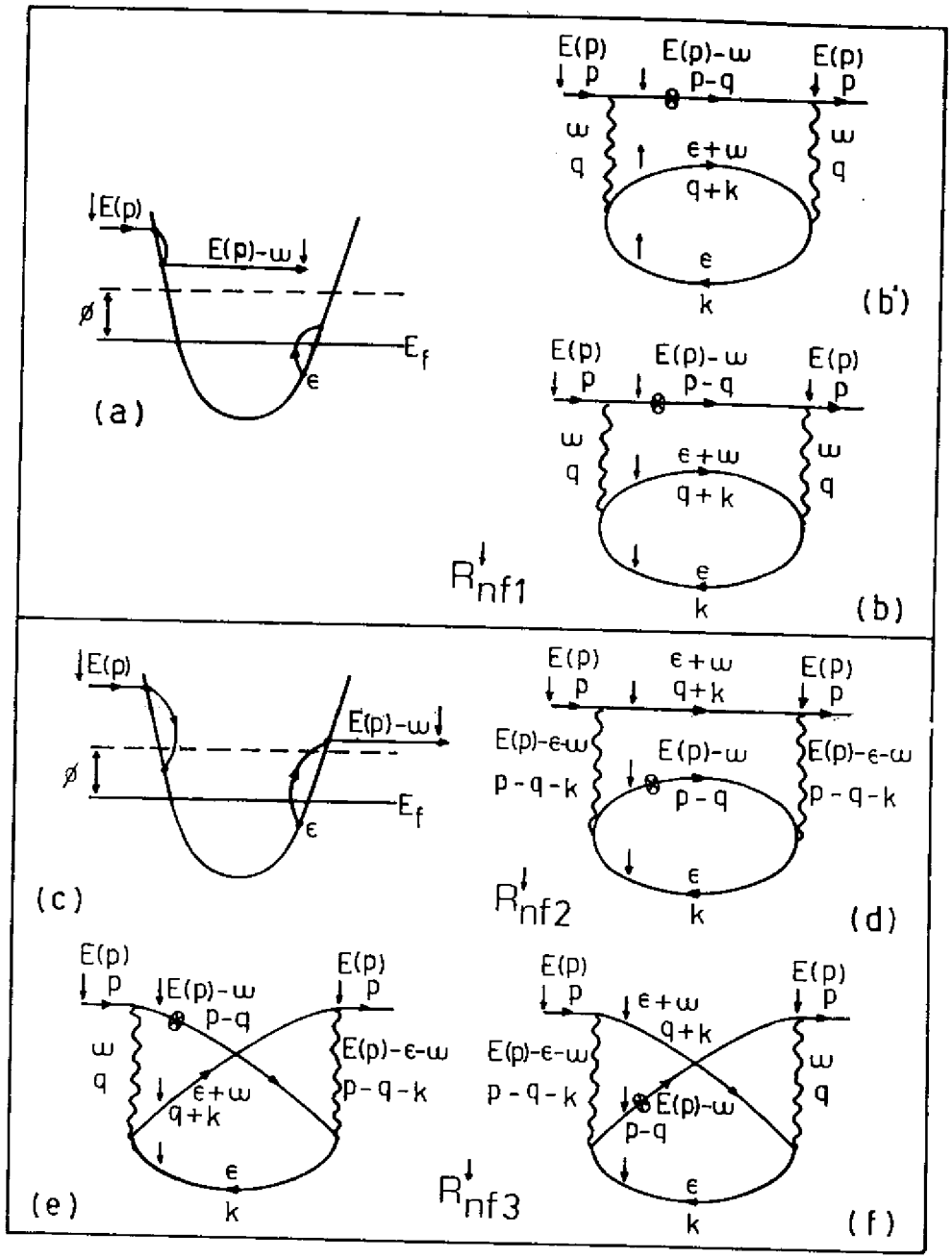
E(p)
E(p)-ω
E_f
ø
ϵ
(a)
E(p)
p
E(p)-ω
p-q
ω
q
ϵ+ω
q+k
ϵ
k
(b')
(b)
$R^{\downarrow}_{nf1}$
E(p)-ϵ-ω
p-q-k
ϵ+ω
q+k
(c)
(d)
$R^{\downarrow}_{nf2}$
(e)
(f)
$R^{\downarrow}_{nf3}$

FIG. 4

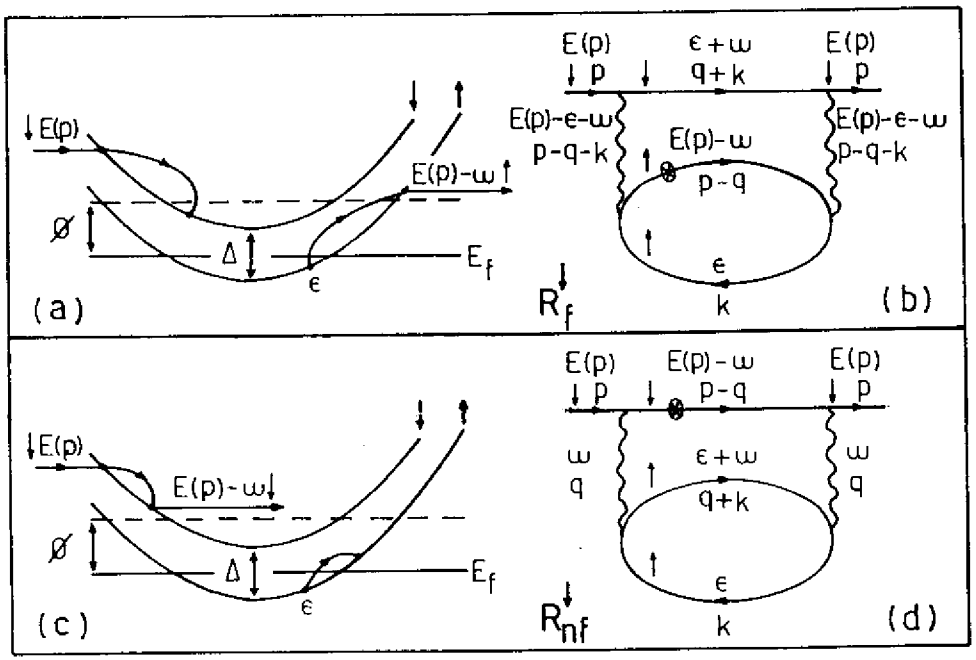
E(p)
E(p)-ω
ø
Δ
ϵ
E_f
(a)
E(p)
ϵ+ω
q+k
E(p)
p
E(p)-ϵ-ω
p-q-k
E(p)-ω
p-q
ϵ
k
R_f
(b)
E(p)
E(p)-ω
p-q
ω
q
ϵ+ω
q+k
R_{nf}
(c)
(d)

FIG. 5

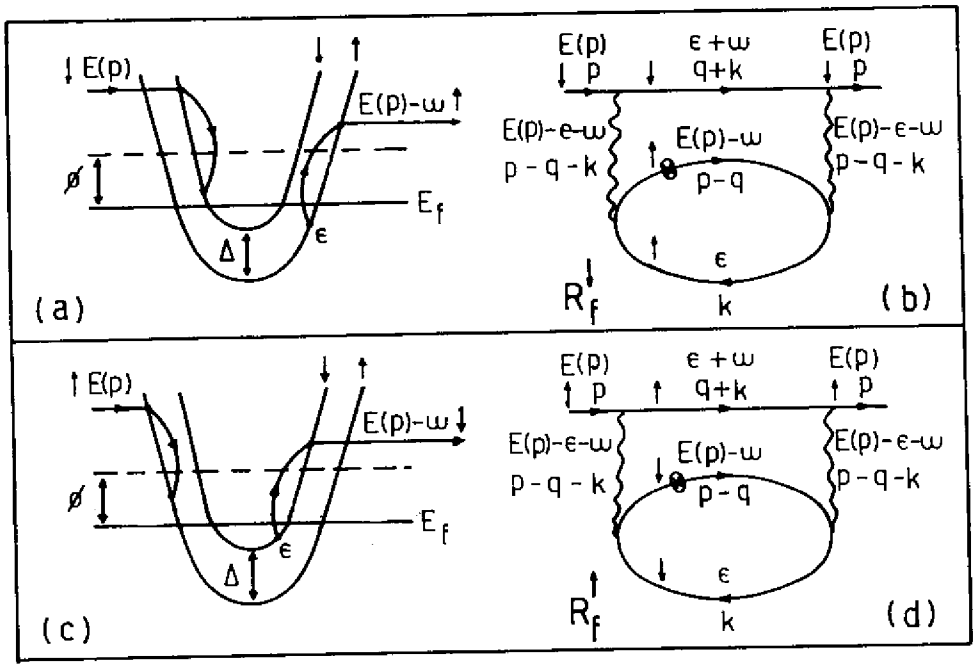
E(p)
E(p)-ω
ø
Δ
ϵ
E_f
(a)
E(p)
ϵ+ω
q+k
E(p)-ϵ-ω
p-q-k
E(p)-ω
p-q
R_f
(b)
(c)
(d)

FIG. 6

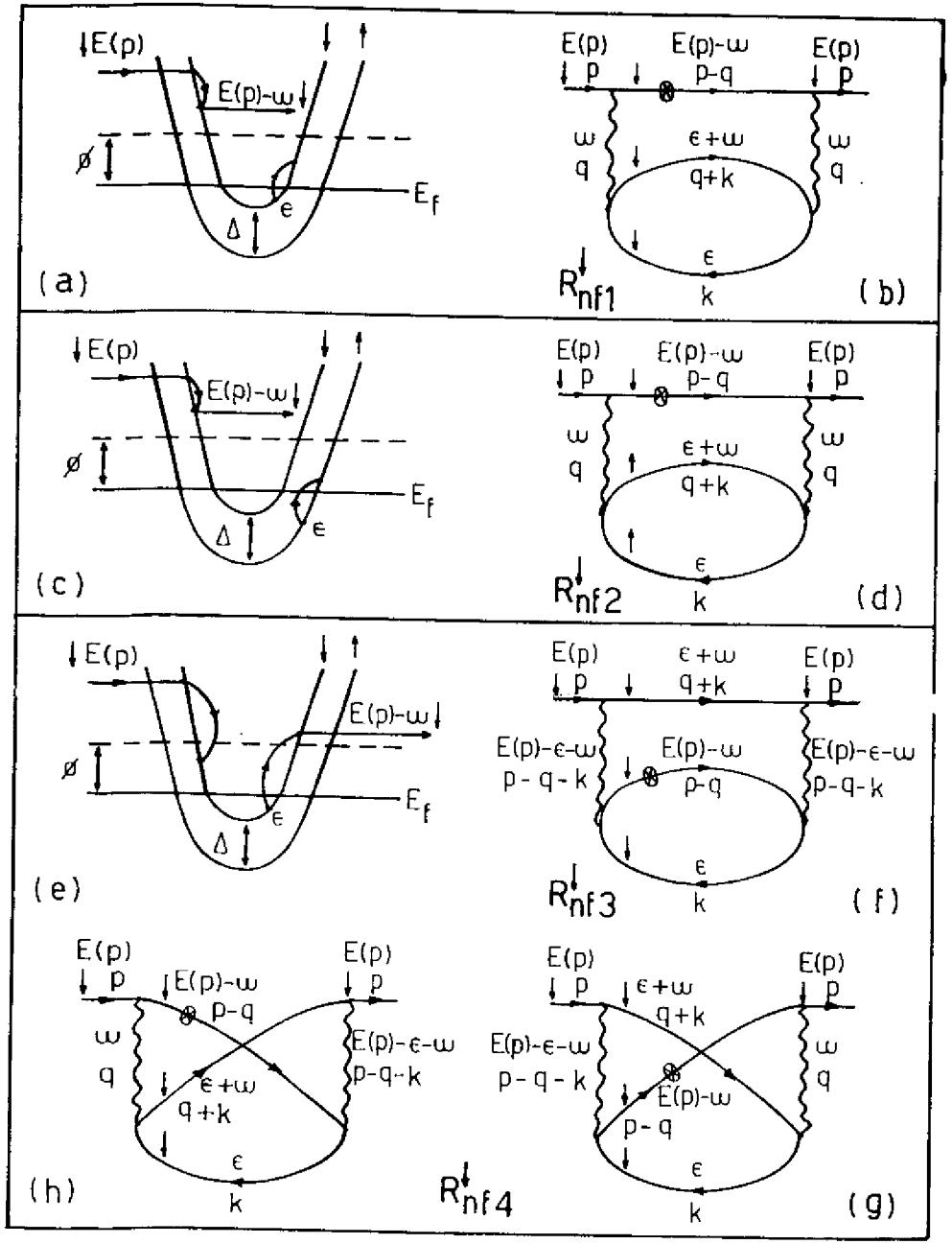
E(p)
E(p)-ω
E(p)-ω
p-q
E(p)
p
ω
q
ϵ+ω
q+k
ϵ
k
Δ
e
E_f
(a)
(b)
(c)
(d)
(e)
(f)
(g)
(h)
E(p)-ϵ-ω
p-q-k
R_{nf1}
R_{nf2}
R_{nf3}
R_{nf4}

FIG. 7

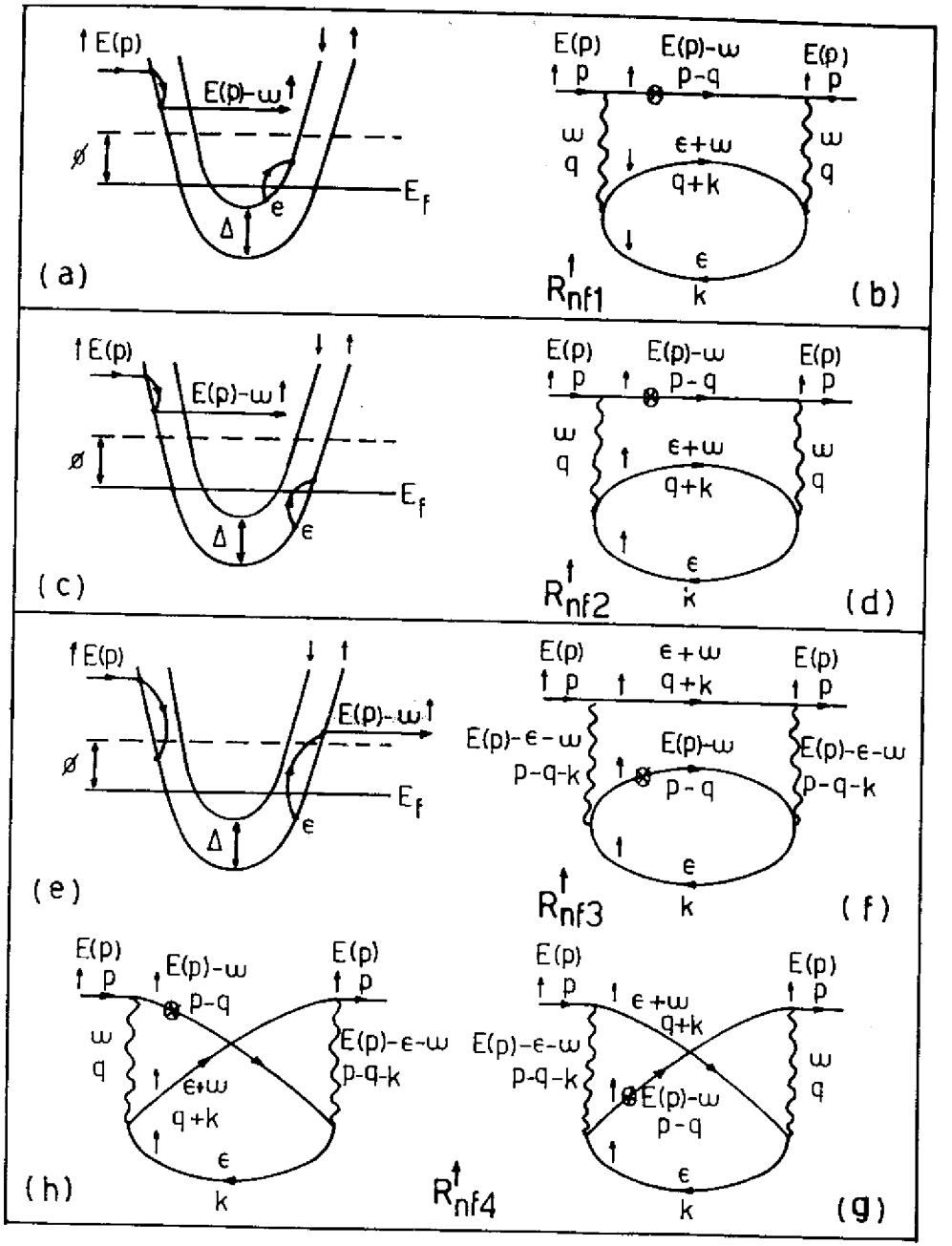
E(p)
E(p)-ω
E(p)-ω
p-q
E(p)
p
ω
q
ϵ+ω
q+k
ϵ
k
Δ
e
E_f
(a)
(b)
(c)
(d)
(e)
(f)
(g)
(h)
E(p)-ϵ-ω
p-q-k
R_{nf1}
R_{nf2}
R_{nf3}
R_{nf4}

FIG. 8

FIG. 9

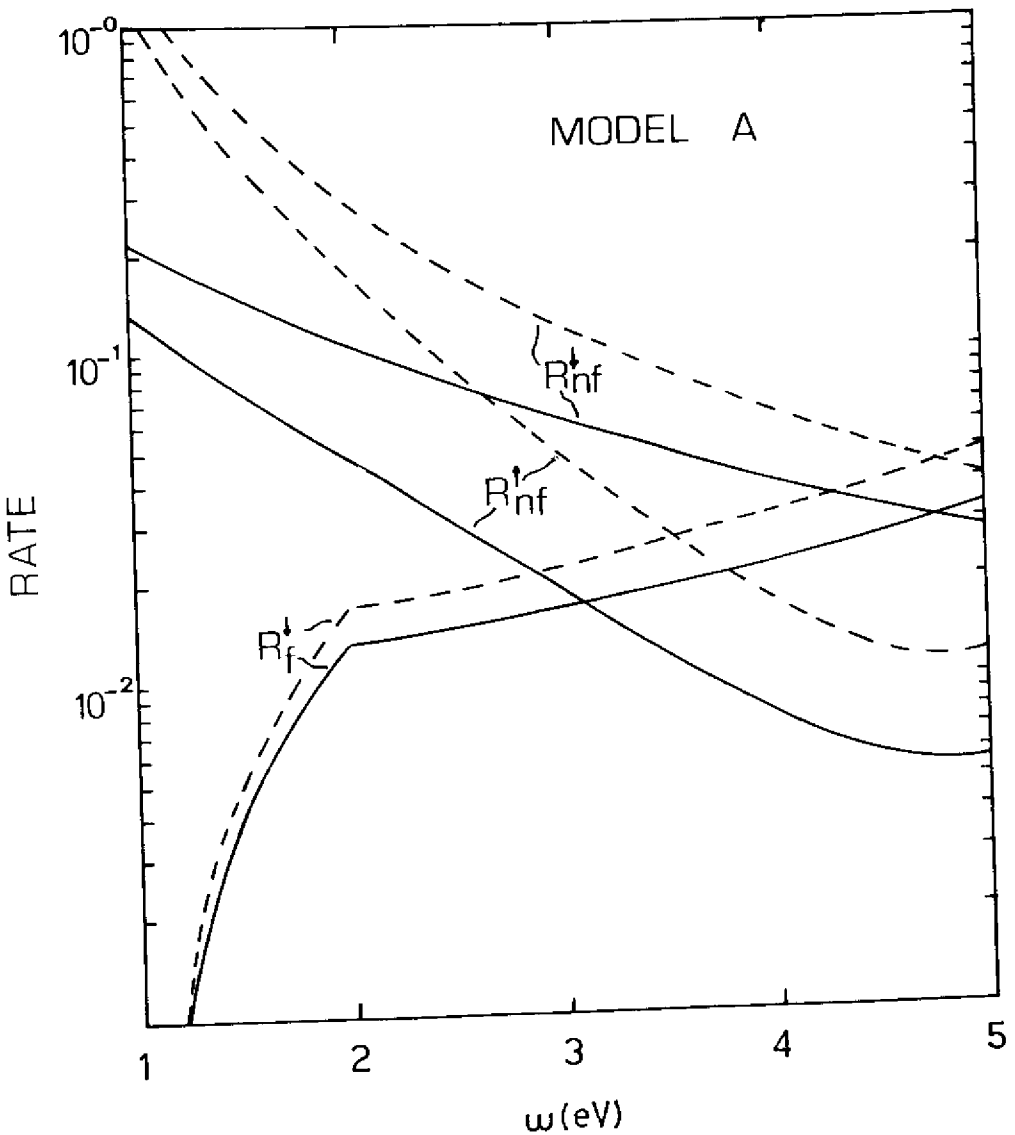
MODEL A
RATE
10^{-0}
10^{-1}
10^{-2}
$R^{\downarrow}_{nf}$
$R^{\uparrow}_{nf}$
$R^{\downarrow}_{f}$
1
2
3
4
5
ω(eV)

FIG. 10

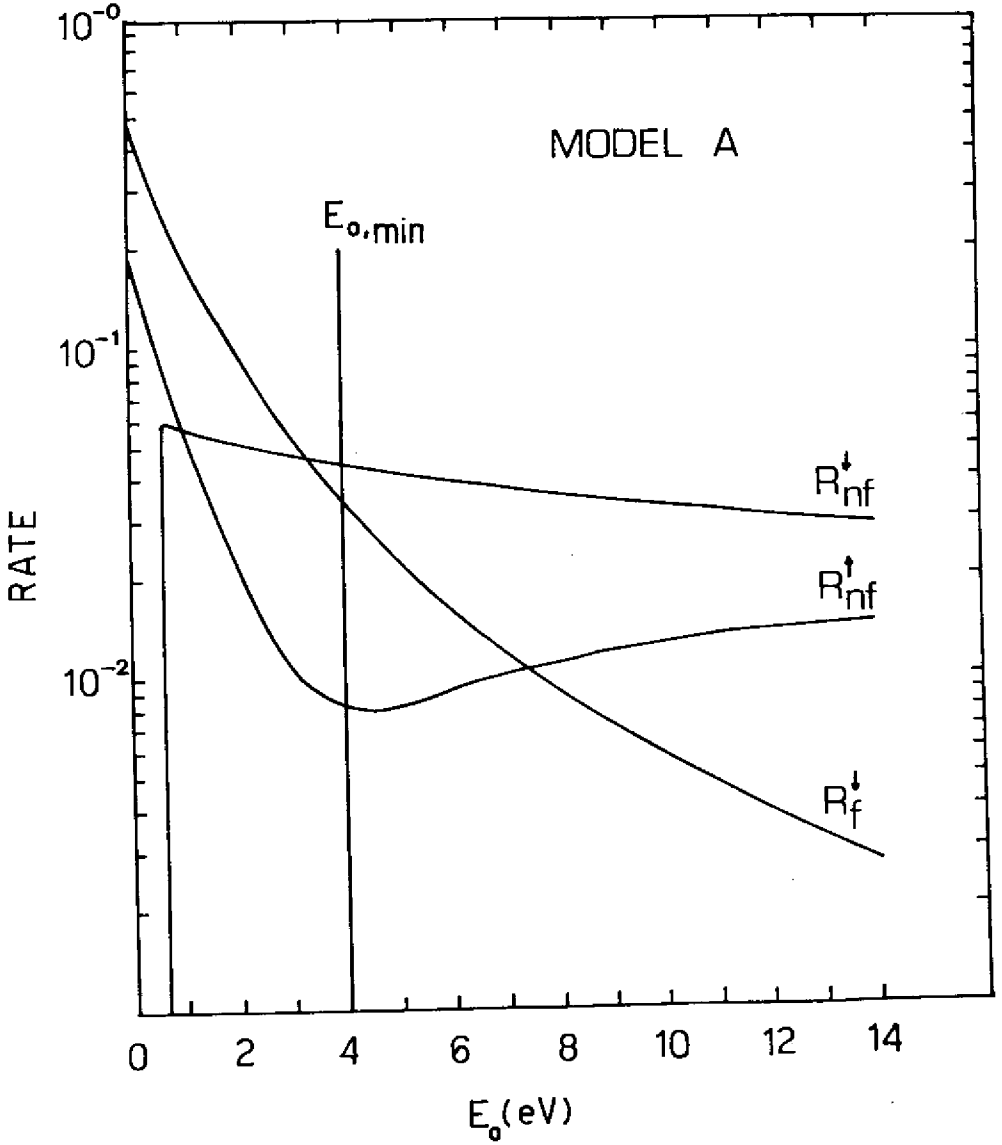
MODEL A
$E_{o,min}$
RATE
10^{-0}
10^{-1}
10^{-2}
$R^{\downarrow}_{nf}$
$R^{\uparrow}_{nf}$
$R^{\downarrow}_{f}$
0
2
4
6
8
10
12
14
E_o(eV)

FIG. 11

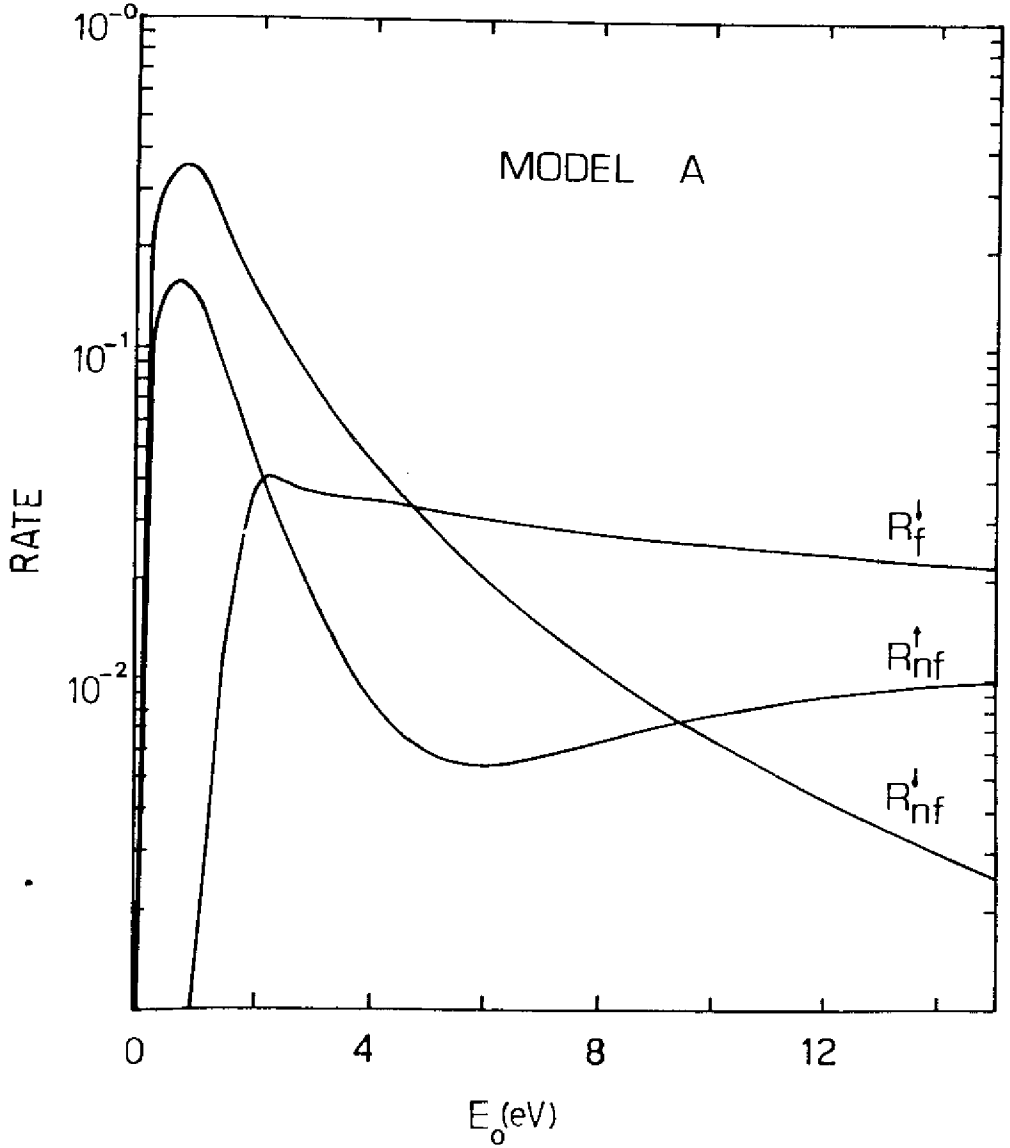
MODEL A
RATE
10^{-0}
10^{-1}
10^{-2}
$R_f^{\downarrow}$
$R_{nf}^{\uparrow}$
$R_{nf}^{\downarrow}$
0
4
8
12
E_o(eV)

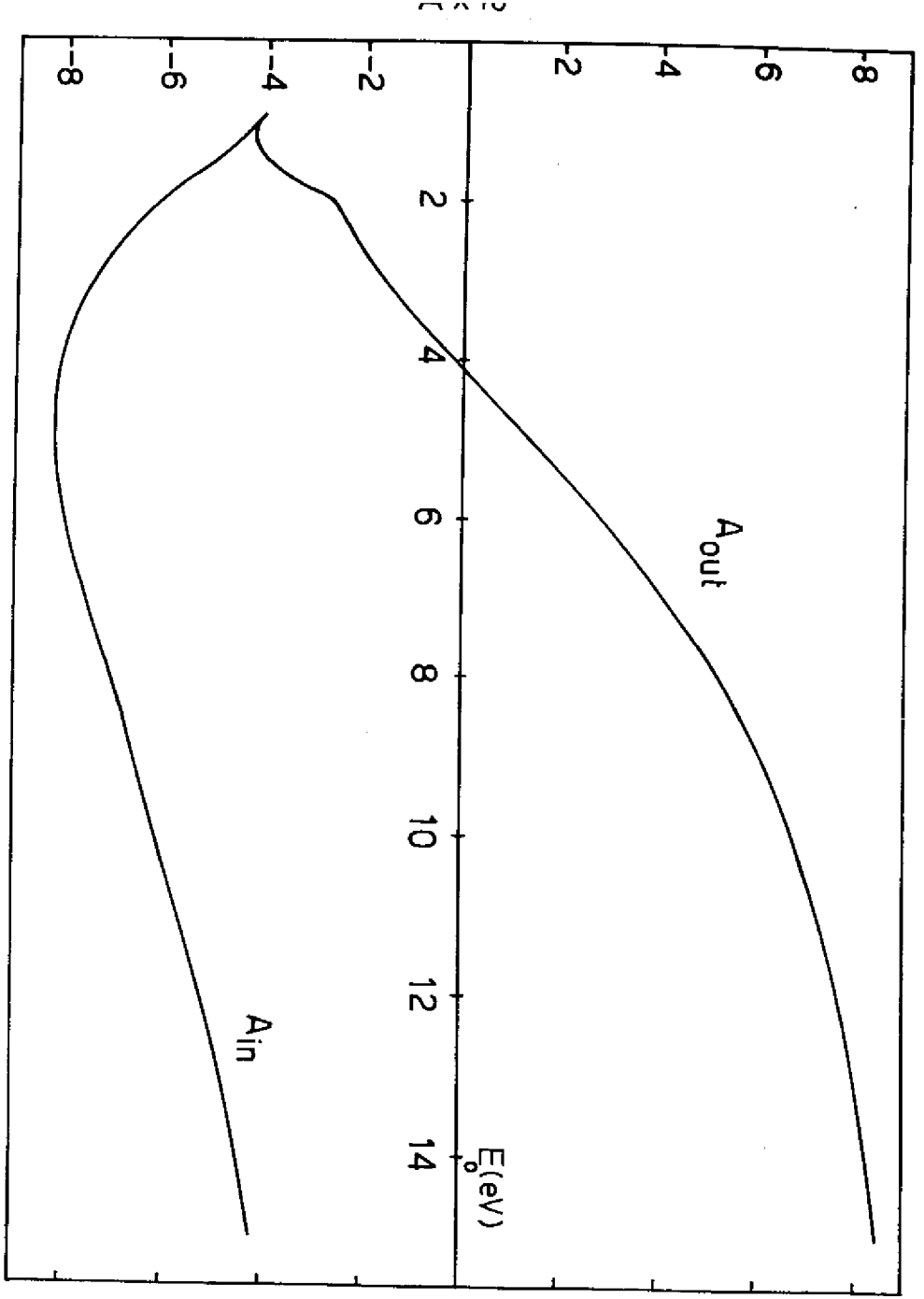
A_{out}
A_{in}
E_o(eV)

FIG. 12

FIG. 13

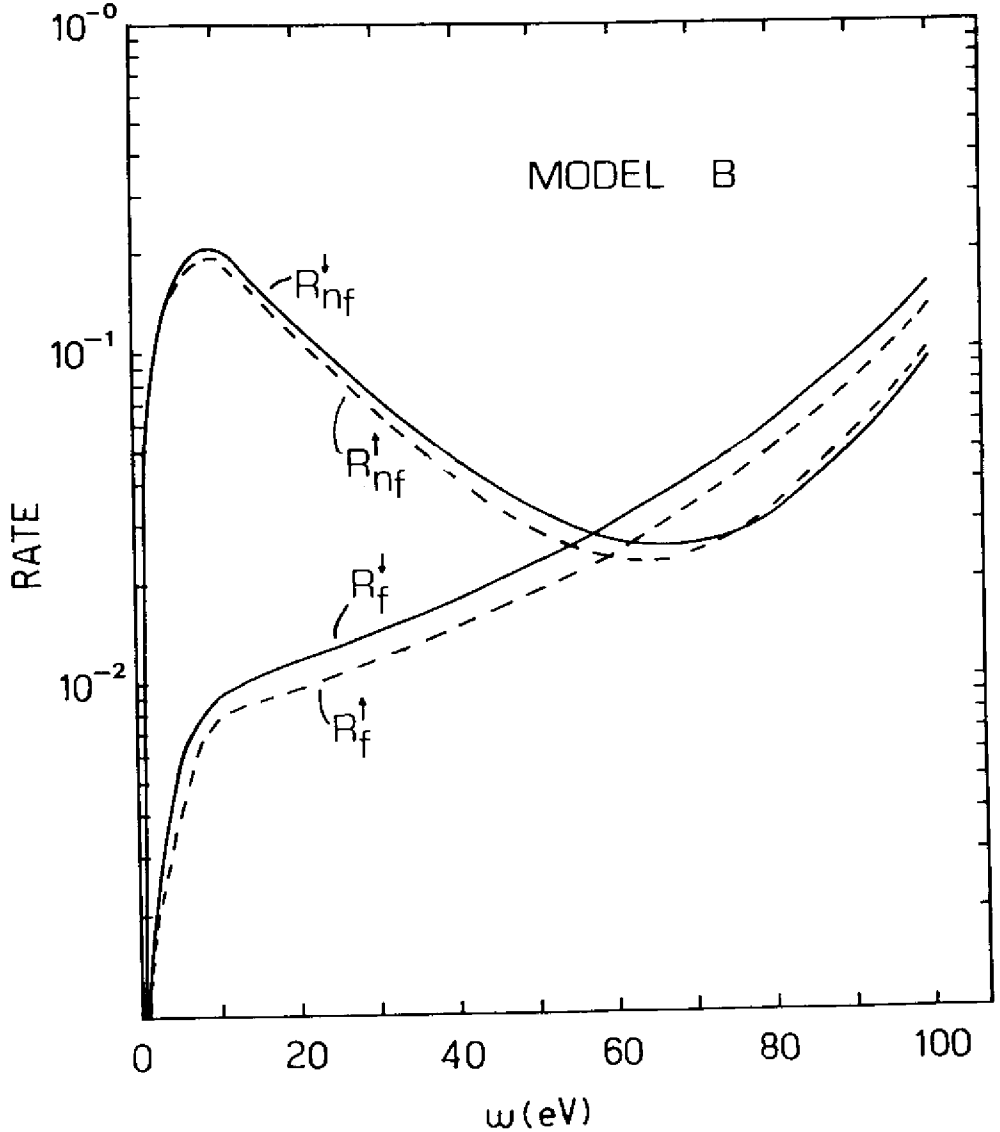

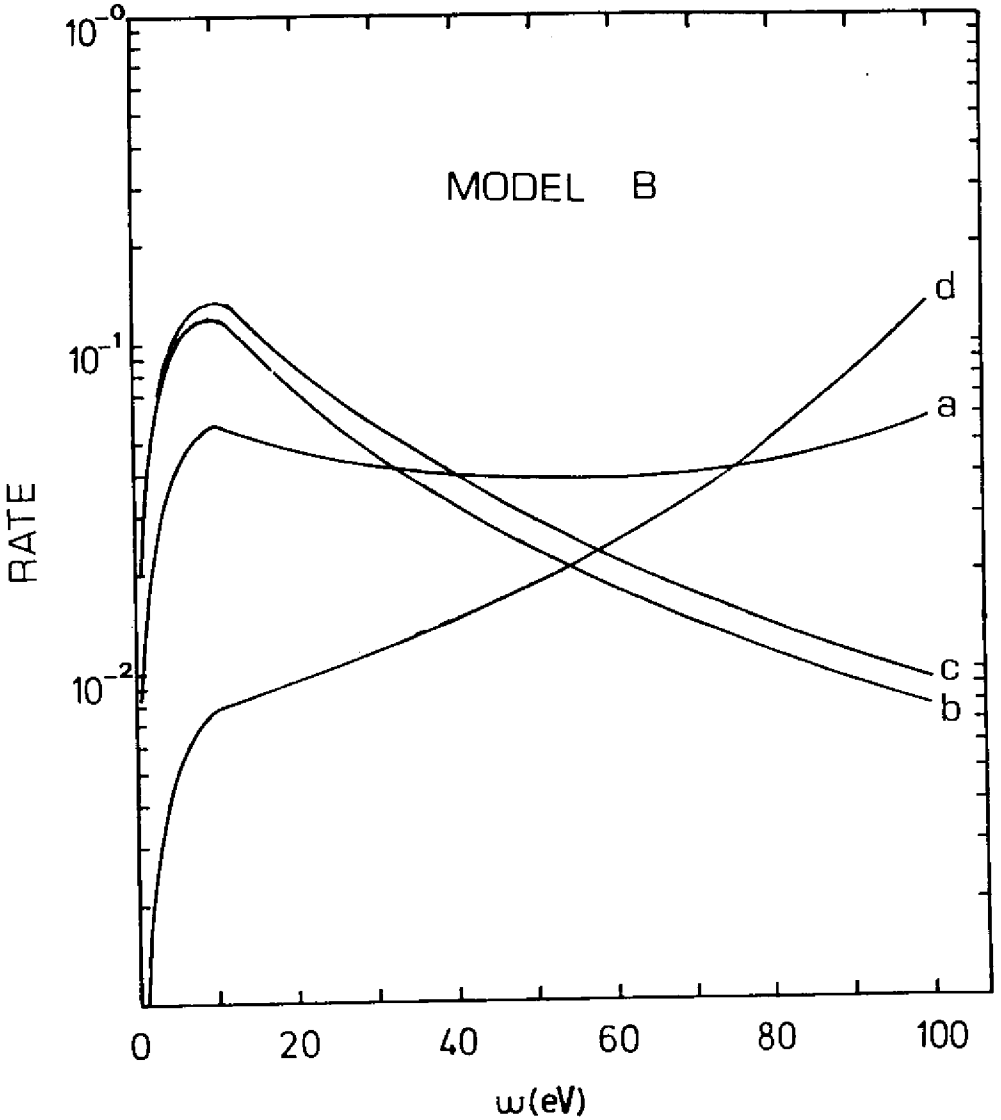

FIG. 14a

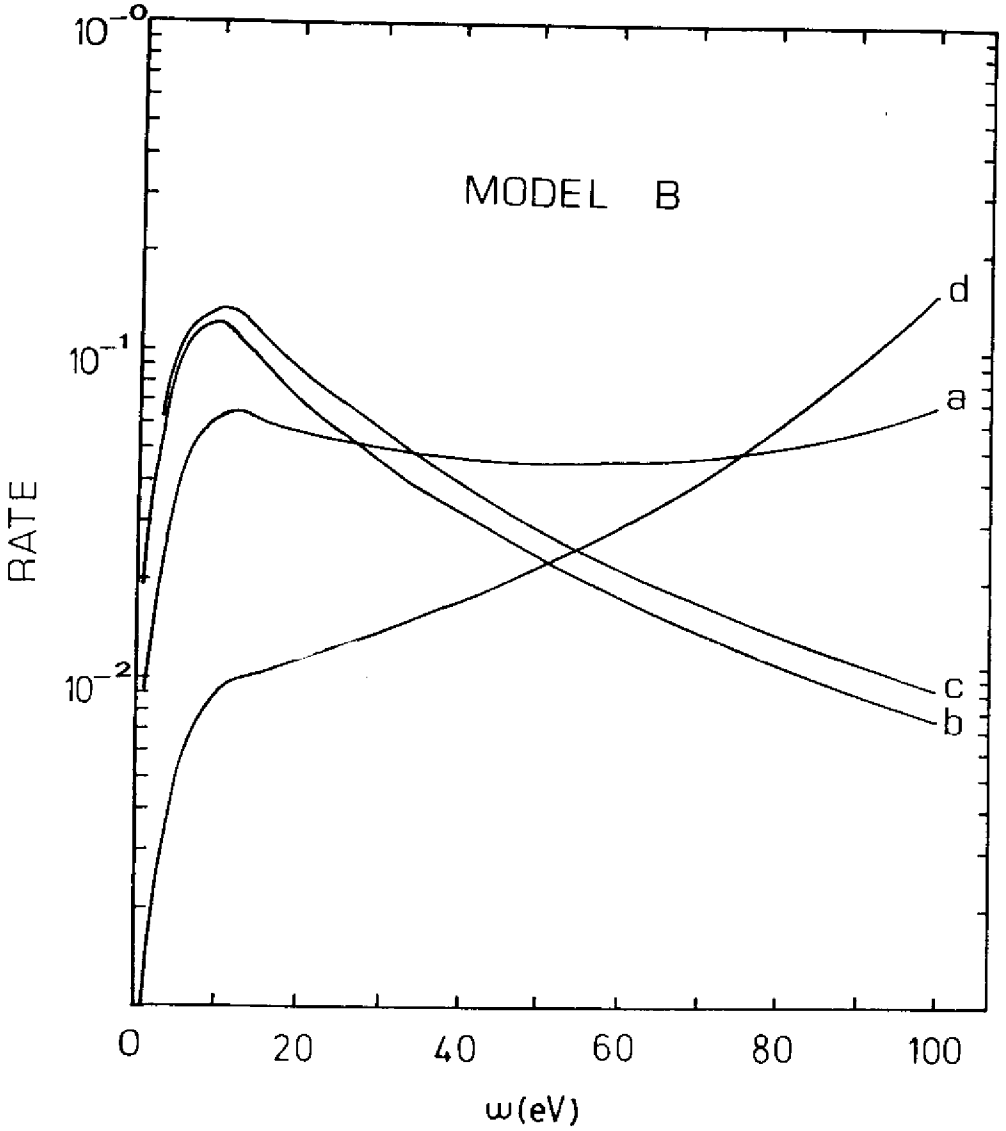

FIG. 14b

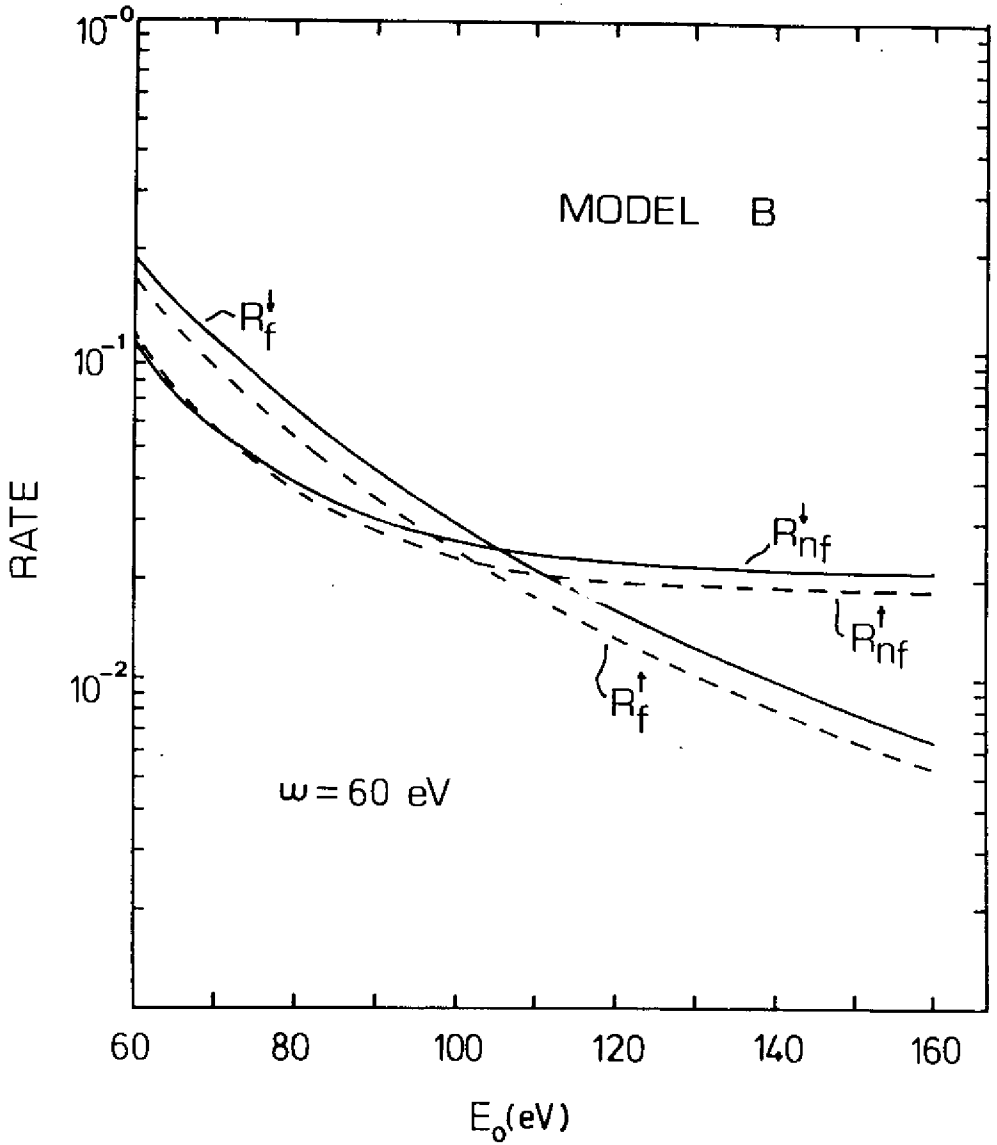

FIG. 15

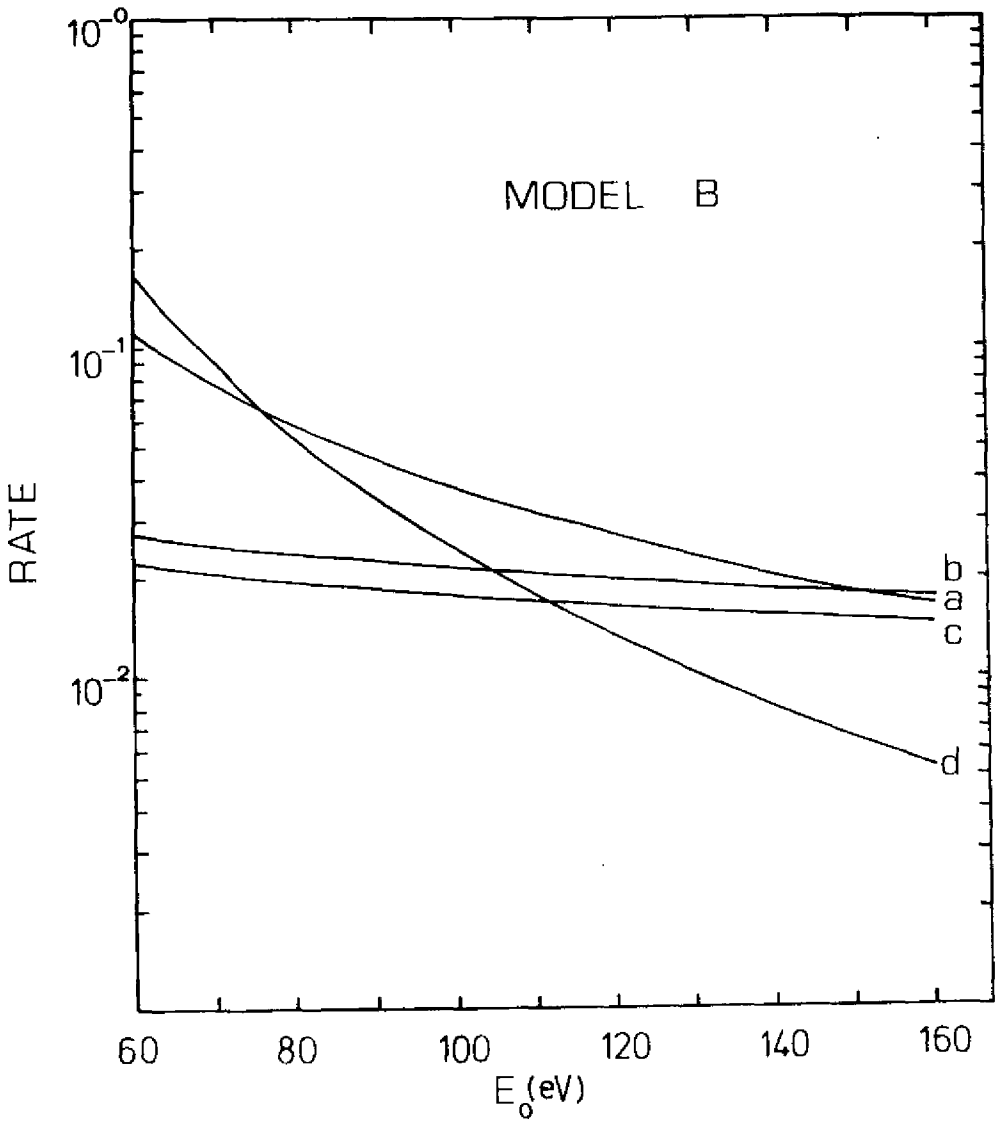

FIG. 16a

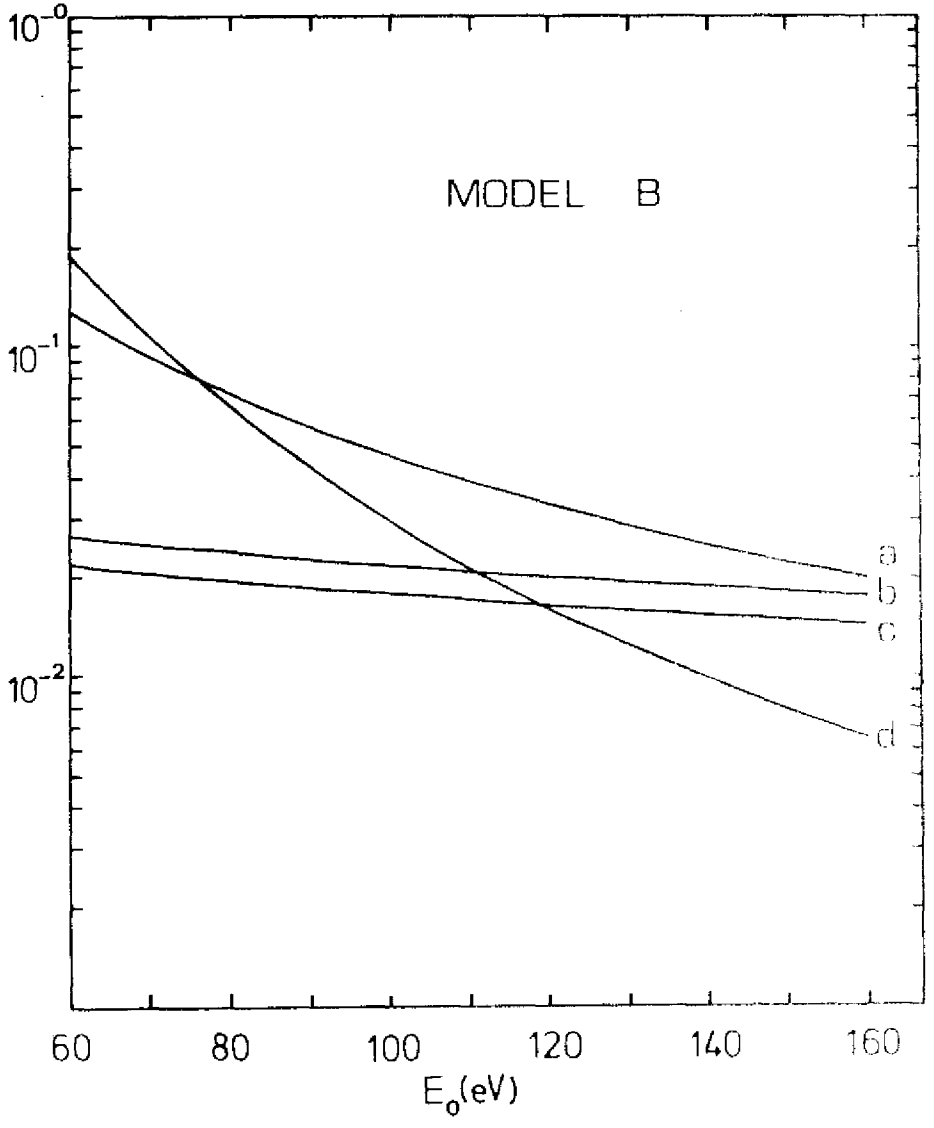

FIG. 16b

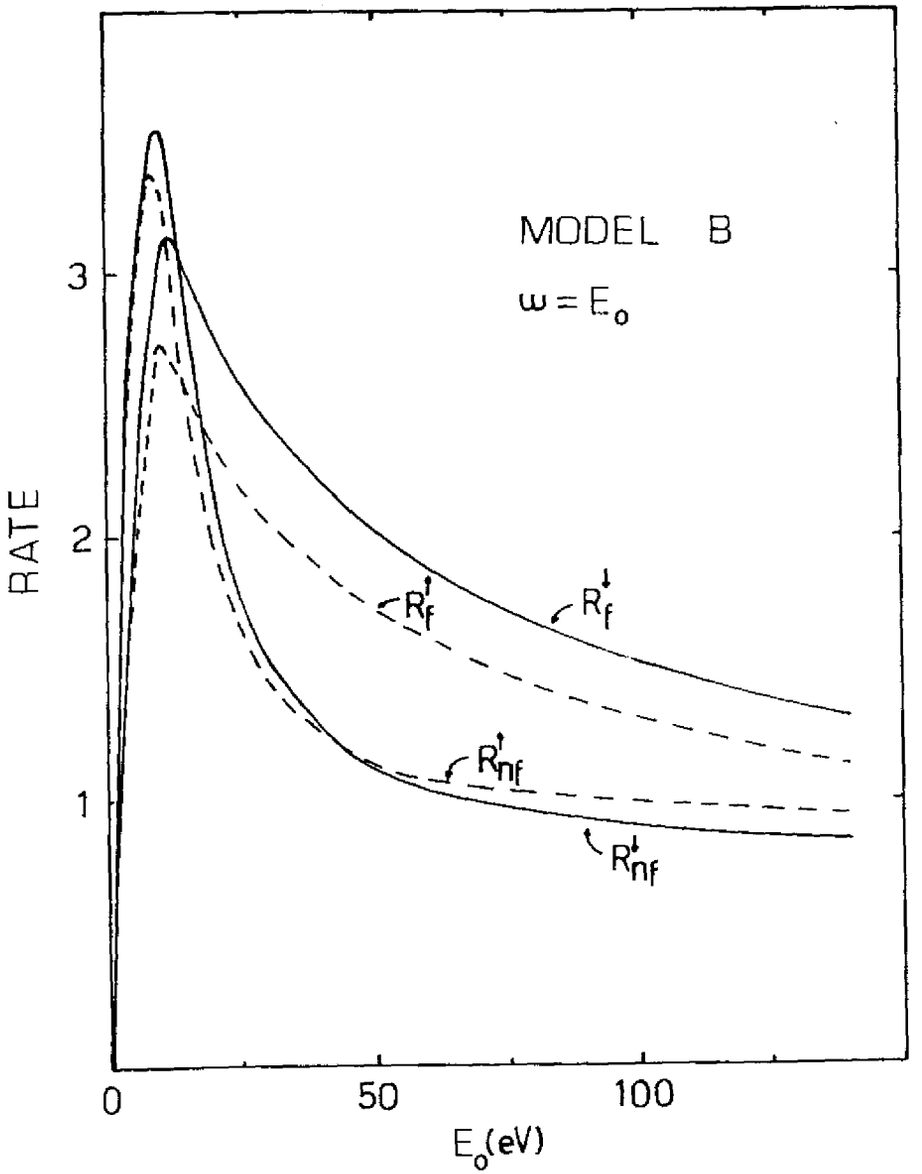
MODEL B
ω = E_o
RATE
3
2
1
0
50
100
E_o(eV)
R↑f
R↓f
R↑nf
R↓nf

FIG. 17

FIG. 18

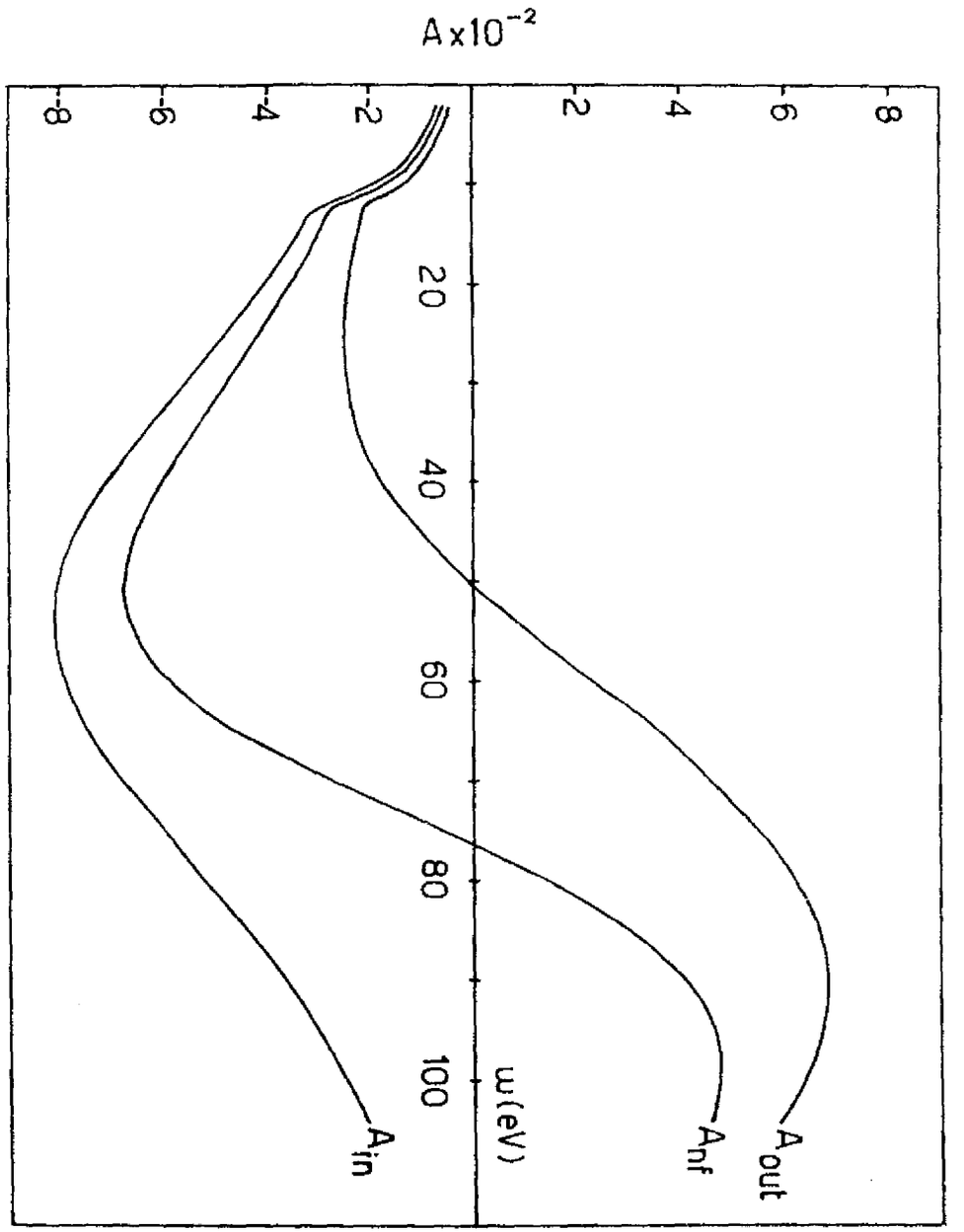
A x10^-2
8
6
4
2
2
4
6
8
20
40
60
80
100
ω(eV)
A_in
A_nf
A_out

FIG. 19

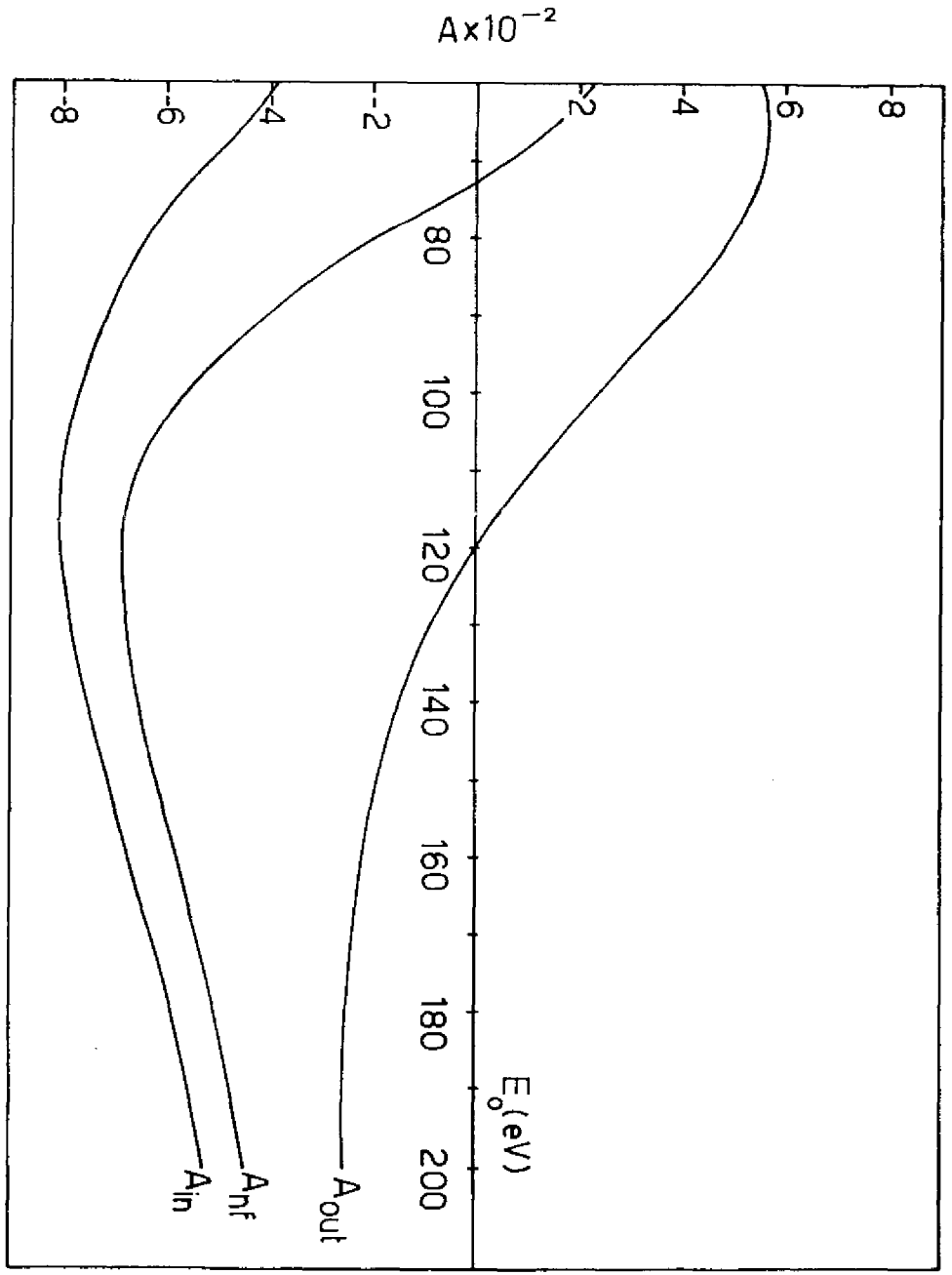
A×10⁻²
-8
-6
-4
-2
2
4
6
8
80
100
120
140
160
180
200
E₀(eV)
A_in
A_hf
A_out

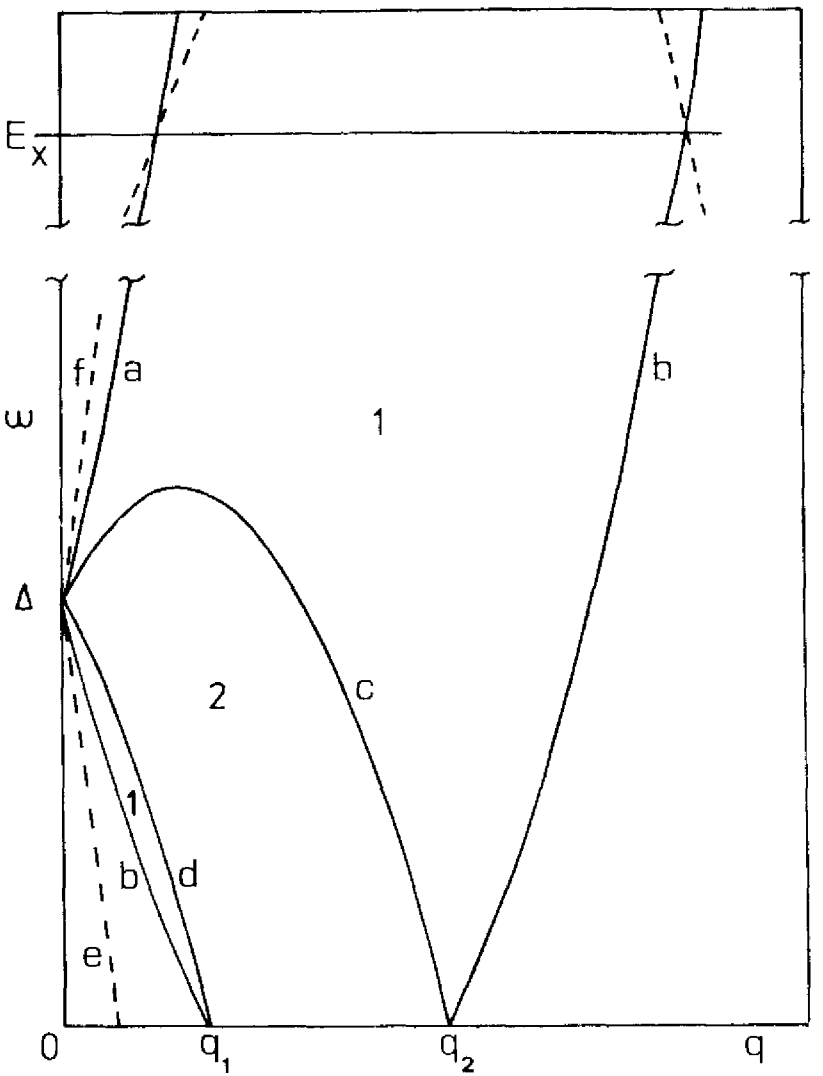
E_x
ω
Δ
f
a
b
1
2
c
1
b
d
e
0
q₁
q₂
q

FIG. A1

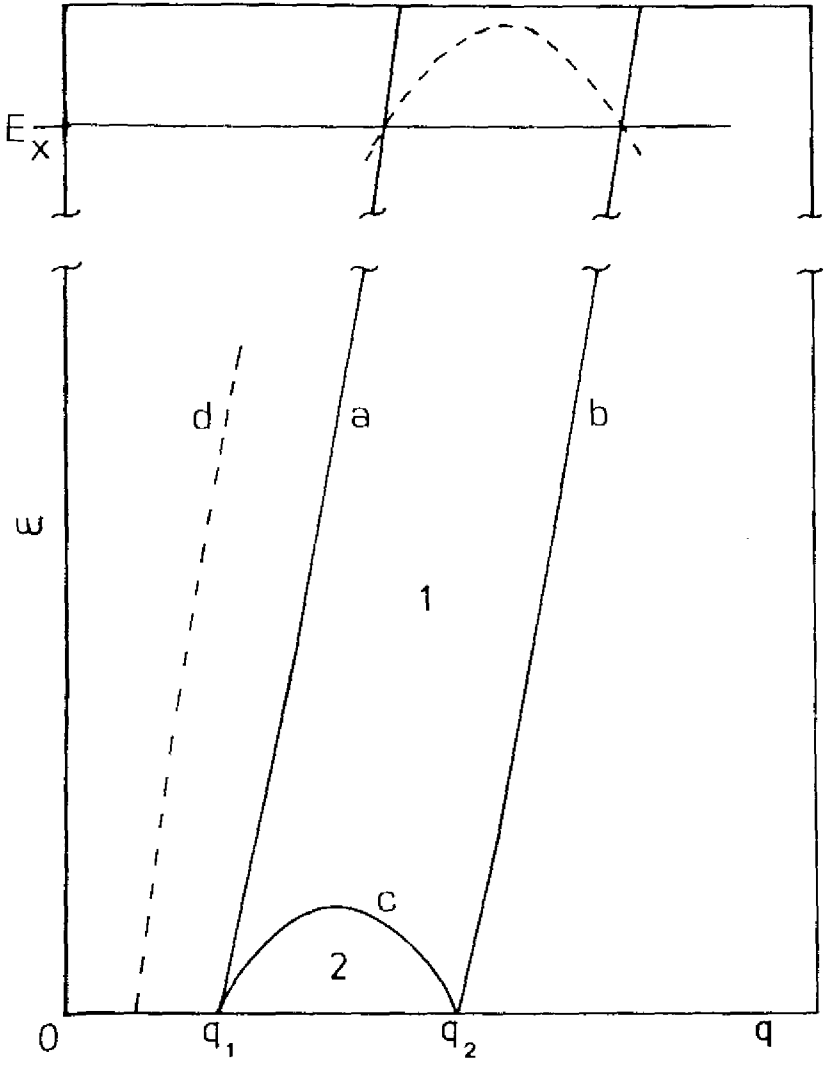

FIG. A2

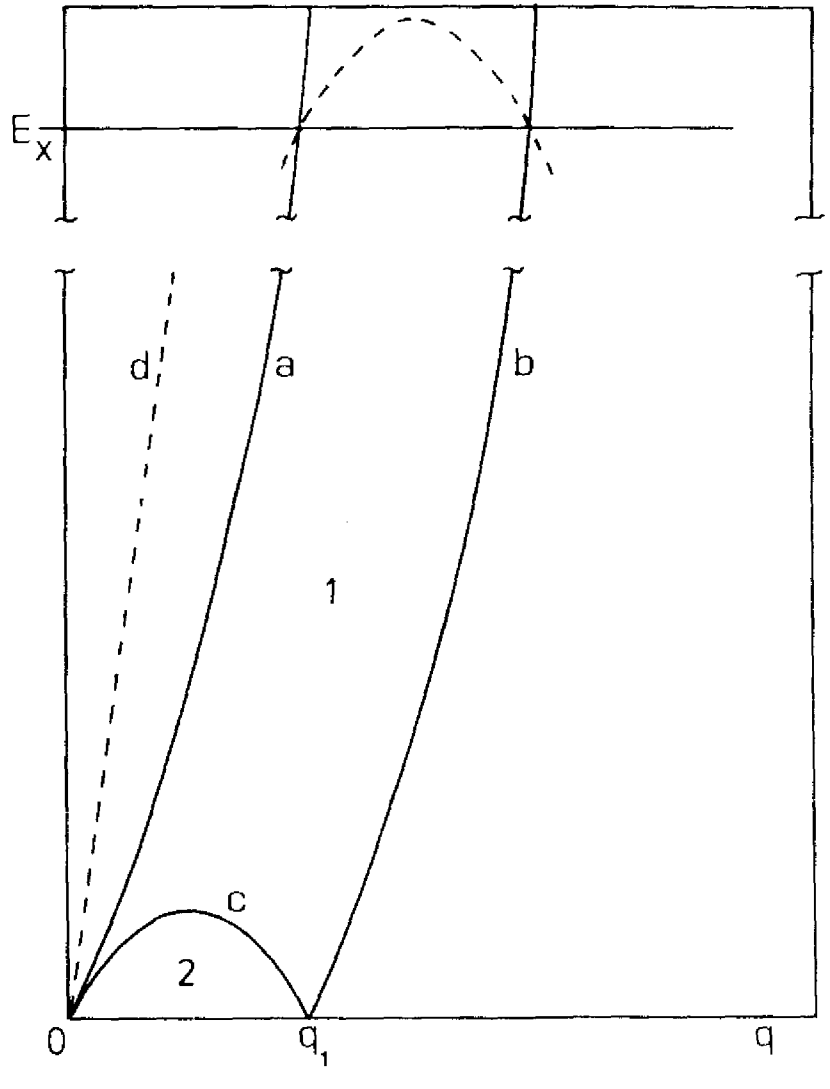

FIG. A3

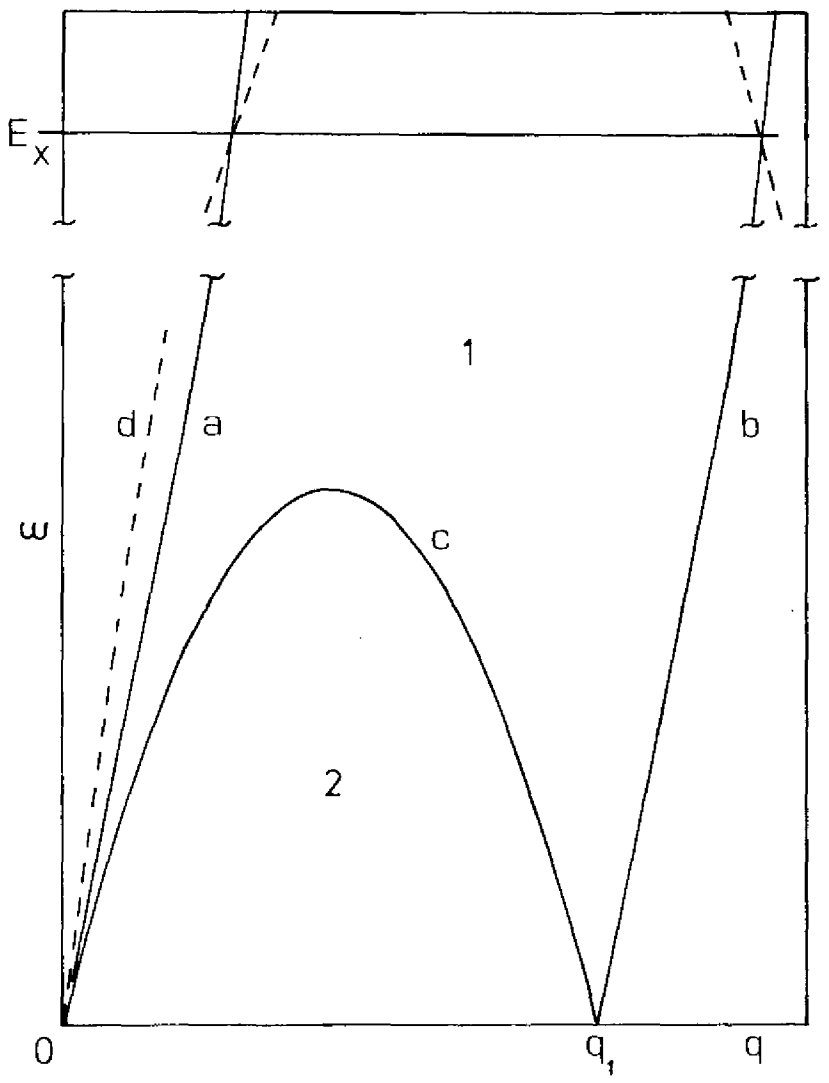

FIG. A4

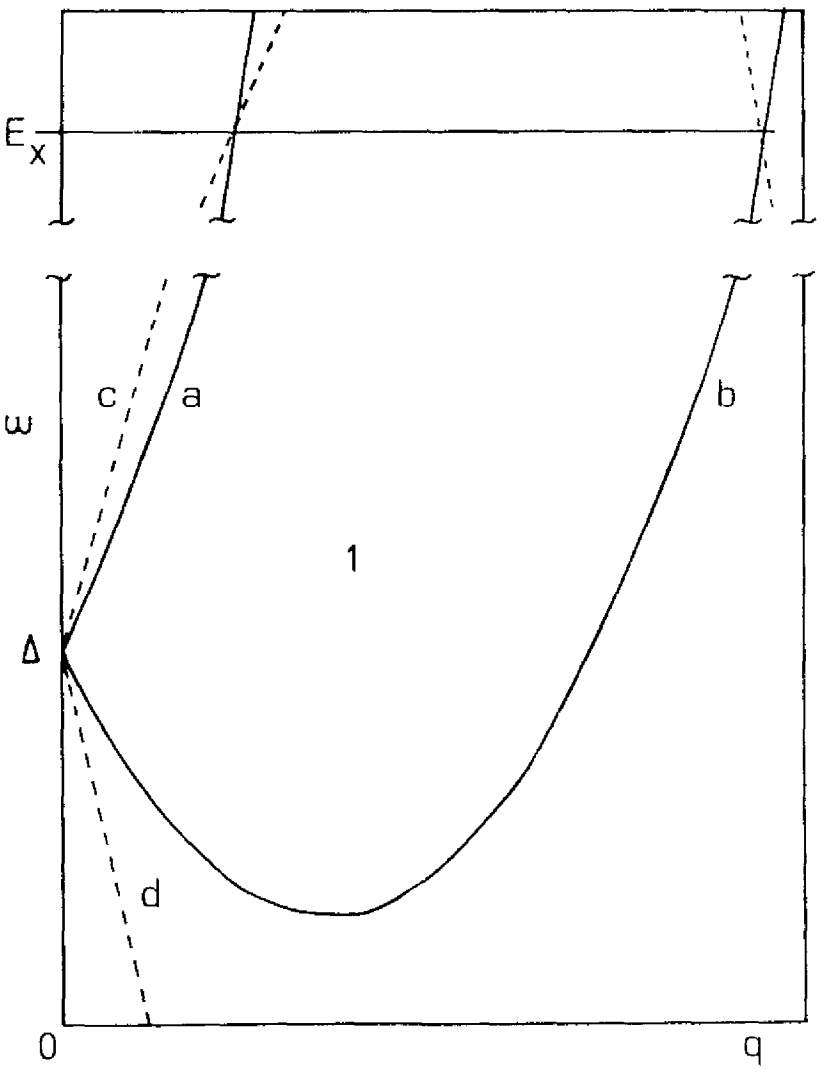

FIG. A5

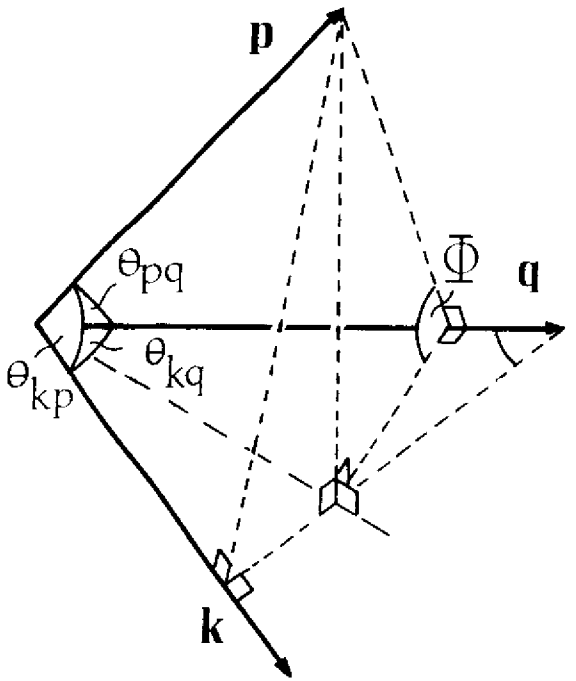

FIG. A6